THERMAL AND SPECTROSCOPIC INVESTIGATIONS

ON POLYMER-BASED

NANOFIBERS

A Thesis

by

OMOSOLA ORIRETAN

Submitted to the Graduate College of
The University of Texas Rio Grande Valley
In partial fulfillment of the requirements for the degree of

MASTER OF SCIENCE

December 2020

Major Subject: Chemistry

THERMAL AND SPECTROSCOPIC INVESTIGATIONS

ON POLYMER-BASED

NANOFIBERS

A Thesis
by
OMOSOLA S ORIRETAN

COMMITTEE MEMBERS

Dr. Mohammed Jasim Uddin
Chair of Committee

Dr. Karen Lozano
Committee Member

Dr. Javier Macossay-Torres
Committee Member

Dr. Mircea Chipara
Committee Member

December 2020

ABSTRACT

Oriretan, Omosola S., Thermal and Spectroscopic Investigations on Polymer-based Nanofibers. Master of Science (MS), December 2020, 81 pp., 2 tables, 50 figures, references 81 titles.

Nanofibers of Poly (ethylene oxide), PEO, Poly (vinylpyrrolidone) PVP, and Co-nanofiber of PEO-PVP were prepared by dissolving PEO, PVP in water. The solutions were added to the PEO solutions, the mixtures were homogenized under mechanical stirring with the aid of magnetic stirrer . The PEO solutions, PVP solutions, and the co-polymer solutions of PEO-PVP were centrifugally spun using Forcespinning™ machine. The obtained nanofibers were subjected to FTIR analysis, and various heating and cooling cycles with heating and cooling rates ranging from 1^0C/min to 60^0C/min using differential scanning calorimetry (DSC 214). The obtained nanofibers were also subjected to Thermogravimetry Analysis (TGA). The research is focused on the effect of heating and cooling rates, phase transitions of PEO nanofibers and their co-nanofibers due to effects of various heating and cooling rates and the spectroscopic investigations on these polymer-based nanofibers.

DEDICATION

The completion of this master degree plan would not have been possible but for the love and the support from my wife ,Orirretan Chukwunedum who relentlessly kept praying for me , my son, David who kept asking me if am in the science laboratory , my daughter, , has been so supportive with prayers and to my youngest daughter that I have not physically seen because I left the shore of Nigeria three months before your birth. I own you all the love and care I could give from a thousand miles away.

ACKNOWLEDGEMENTS

I will be grateful to Dr. Mohammed Jasim Uddin, chair of my dissertation committee, for all his mentoring and advice; he kept telling that I should go ahead. For my research adviser, Dr Mircea Chipara, your patience and fatherly approach for the success of this degree plan can never be over emphasized. He kept encouraging me , directing me to the next successful steps all through the experimental procedures, writing and editing this manuscripts. My gratitude go to my dissertation committee members: Dr.Karen Lozano, you are a great mother,mentor and you are always there to give supporting ideas, information for the success of this manuscript, Dr. Javier Macossay-Torres, who is also the chemistry graduate coordinator has been so supportive in ensuring that my presentation and manuscript are well presented. Your advice and comments have really helped this far. I want to also thank the Graduate college for award, Presidential Graduate Research Assistantship , given to me. The award took care of my tuition fees and stipends and this contributed to my success in this manuscript.

I would also like to thank Carlos Delgaldo, an undergraduates who volunteered his time to assist me with these projects.

TABLE OF CONTENTS

Page

LIST OF TABLES

Page

LIST OF FIGURES

Page

CHAPTER I

INTRODUCTION

Poly (ethylene oxide), PEO, is a unique type of polymer because of its solubility in both water and some organic solvents. This unique property of PEO has been harnessed in so many applications such as in areas of drug delivery, wound dressing[1], tissue engineering scaffolding[2], filter media[3], thermal sensor[4], energy storage[5],piezoelectric sensor, protective clothing[6] and cosmetic skin mask[7].

These applications of PEO based polymer, nanofibers and their nanocomposites have attracted attention on the enhancement of the physical properties of PEO based polymer, PEO nanofiber and PEO nano composite by studying the thermal behavior of PEO, polyvinylpyrrolidone (PVP) and PEO-PVP co-nanofibers .The thermal analysis is a technique that measure a materials response to be heated or cooled to ascertain the relationship between temperature and physical properties of polymer[8] and polymer based nanofibers. Thermal analysis is important part of polymeric materials analysis in the research, development and quality control used in the manufacturing of polymeric materials. The thermal properties are study through the use of Differential Scanning Calorimetry (DSC) and also accompanied by the thermal stability of PEO using Thermogravimetry analysis (TGA).

PEO, PEG and POE are chemically synonymous because they are polymer of polyethylene oxide. PEO has been more acceptable name for polymer of ethylene oxide. PEO exists in both liquid and solid forms depending on the molecular weights. The different molecular weight,

which have different physical properties, determines the different field of application of this polymer. It was reported that the molecular weight and concentrations gave beads, beaded fibers and complete fibers formations due to different degree of molecular entanglement[9].

PEO(PEG) was first reported in 1859.A.V. Lourenco and Charles Adolphe Wurtz individually isolated compounds that were PEG[10]

Polyvinylpyrrolidone (PVP) is a water-soluble(because it binds well to polar molecules, due to its polarity) polymer made from the monomer N-vinylpyrrolidone. It has some many uses. It has been used as a binder in pharmaceutical industry[11]. PVP possesses disinfectant property when is made to react with iodine[11]. Complex of PVP in solution is used in ointment, soap, surgical scrubs, emulsifier, and tooth whitening.

The PEO, PVP nanofibers and PEO-PVP co- nanofibers were produced through Forcespinning™ method (centrifugal force).This uses high-speed rotatory spinneret in which the polymer solutions or melt form jet that stretches ,as the jet stretches ,the solvents evaporate and is the jet is deposited on collector as nanofibers[12].A review on other methods of fabricating nanofibers showed that centrifugal spinning gave high yield of nanofibers at low cost[13]

The nanofibers are obtained from the polymer solution through Forcespinning[12] of the polymer solution uses centrifugal force which is being used to produce nanofibers at high production rate instead of the electrical forces. Key parameters such as solution concentration, rotational speed of the spinneret and collection system are critically considered so that geometry and morphology of nanofibers of interest are obtained. Surface tension and viscoelasticity of the solution are parameters that influence the formation of beaded fibers[14]. Surface tension as a

factor has been reported to cause fiber to break up into droplets before the fiber jets get to the collectors[15]

The as obtained nanofibers are subjected to Raman spectroscopy which provides information on the structure (composition, stress/strain state, crystal symmetry and orientation, quality of the crystal) of the nanofibers. Fourier Transform-Infra red Spectroscopy (FTIR) provides information about the functional groups in the nanofibers. SEM reveals the external morphology and topology of the nanofiber from the signals of the electron scattering off the surface. TGA measures weight/mass change and the rate of change as function of temperature, time and atmosphere which provides information that helps in nanofiber selection for certain end use application. DSC provides information on phase transitions of the nanofibers.

Phase transition: This is equally called phase change between solid, liquid and gaseous state of matter. Certain properties of a given medium change because of the change in external conditions which are mostly temperature and pressure. The measurement of these external conditions at which the transformation occurs is called Phase transition. The glass-transition temperature depends on the heating rate according to a Williams-Landel-Ferry like equation[16].

The PEO, PVP nanofibers and PEO-PVP co- nanofibers were produced through Forcespinning™ method (centrifugal force).This uses high-speed rotatory spinneret in which the polymer solutions or melt form jet that stretches. As the jet stretches ,the solvents evaporate and is the jet is deposited on collectors coupled with the Forcespinning machine as nanofibers[13], [12].A

review on other methods of fabricating nanofibers showed that centrifugal spinning gave high yield of nanofibers at low cost[17].

CHAPTER II

LITERATURE REVIEW

Applications of Polymer Nanofibers

Polymer nanofibers and their nanocomposites importance cannot be over-emphasized because of their applications in the areas of tissue engineering scaffolding; surface of biopolymer was functionalized with carbon nanotubes to form nanoscale topography for treatment of inflammation, angiogenesis and bone regeneration[18]. It was proved that poly(lactide-co-glycotide) (PLGA) was fabricated to nanofibrous state for the support of nerve regeneration capability because of its enhanced surface area and good mechanical properties which gave one directional cells alignment[19].Nanofabricated cultured cell on PLGA that behaved like the native tendon tissue which supported the attachment and penetration of multicomponent ADSCs was made to proof the tendon regeneration process of polymer nanofiber[20]. Electrospun Chitosan Poly(vinly alcohol) has been proved to be biomaterials for the substitution of dermal for would healing[21]. Biodegradable zein-polydopamine polymeric scaffold functionalized with TiO2 nanoparticles has been investigated through in vitro and in vivo as a cheaper biomaterial for skin tissue engineering applications[22].Bioactive material scaffold was fabricated through electrospinning for the delivery of bromelain and salvianolic B for the enhancement of would healing which the potency was confirmed through the in vitro and in vivo chicken chorioallantoic membrane analysis[23]. Biodegradable and biocompatible engineered Type 1 collagen-PEO nanofibers were electrospun to produce nanocomposite that had the ability to used in would healing and tissue engineering system[24]. Solutions that contained chitosan, PEO and

triton X-100 was electrospun to produce cellular compatible aligned nanofibrous matrix that have drawn attention for tissue engineering[25].

Polymer nanofibers fabricated to form polymer nanocomposites have also find applications in the areas of energy storage; Nanofibers composite of $BaTiO_3$ with high aspect ratio was fabricated with surface modification by poly(vinyl pyrrolidone) PVP which was used as filler for Poly(vinylidene fluoride-hexafluoropropylene) (PVDF-HFP) demonstrated higher discharged energy density than the commercial available biaxial polypropylene[26]. A fabricated polymer nanofibers of $BaSrTiO_3$ filled with PVDF having large aspect ratio and enhanced crystallinity gave an output of maximal energy density[27]. A co-electrospun 3D nanohybrid that consisted of nano oxide of manganese was fabricated with graphene to form a nanohybrid that demonstrated enhanced capacitances[28]. Carbon nanofibers of high surface areas were doped with SiO_2 and these were successfully used as anodic electrode in lithium-ion battery having shown better cyclic stability, charge-discharge kinetics and stable storage ability[29]. Electrospinning was used to fabricate nanofiber composite of poly(vinylidene fluoride) and SiO_2 as membrane for interconnection of pores, it was reported that good ionic conductivity and high porosity of electrolyte was achieved[30]. A functionalized multiwall carbon nanotubes were fabricated with thin fil electrode of polyaniline that gave a great electrochemical result with high energy density and capacitance for energy storage.[31]

Polymer nanofibers have also gained importance in the area of protective clothing; Protective clothing is classed as set of clothing that protect the body from physical damage, nuclear assault, biological exposure, chemical incident, fire incident, and cold environment .Electrospun nylon 6

polymer was functionalized with MgO nanoparticle to produce fire retardant and anti-bacteria protective clothing[32].Layered fabric for agricultural purpose was made with polyurethane and the barrier efficacy was confirmed by the ability of the nano fabricated fabric layered to disallow the penetration of pesticide[33].High performance material, Kevlar, and aromatic polyimide nanofibers were successfully fabricated for protective clothing against heat and fire and the thermal stability and fire resistance of these fabricated materials were confirmed by thermogravimetric analysis[34]. Nanoparticles made from metal oxides such as MgO, Al2O3,FeO3,ZnO and TiO2 have been confirmed to reduce the potency of chemical and biological warfare agents by degrading these agents into non-toxic products and these properties erred these metal oxides the ability to be used in protective clothing[35].

Polymer nanofibers have also been used in filter media which have their surfaces been modified to improve filtration efficiency ; Polystyrene nanofiber mixed micro glass for modification of the media has been used to separate water droplets from emulsified oil in the petrochemical industries to boost the performance of the micro glass media filter[36].Polyamide 6 and Polyamide 6/6 nanofibers were successful electrospun for filtration of air due to the smallest diameter obtained from the fabrication of these nanofibers[37]. Polymer nanofiber of polyvinyl acetate and polyvinylpyrrolidone were fabricated to morphology of interpenetrating network nanofibers for separation of water droplets from very low Sulphur diesel mixture[38] .Nylon 6 polymer solution was electrospun to a superhydrophilic bilayer with cellulose membrane, this structure was successfully demonstrated high performance in water filter media[39].Polyurethane cationomers were fabricated using electrospinning method to produce nanofibers of different

loading of quaternary ammonium groups for antimicrobial filtration against staphylococcus and Escherichia coli[40].Nano-fibrous of polyacrylonitrile was treated with hydroxylamine to form a coordinated silver compound after reacting with silver nano particles which has a high tendency of killing microorganisms and this potential has been used to develop antimicrobial filters for water and air[36]. Polylacticide/polyhydroxybutyrate and various amount of ammonium-based ionic liquid were elecrospun to fabricate nanofiber that was successfully used in aerosol particle filtration.

Methods of Fabrication Polymer nanofibers

There are many methods of fabricating nanofibers and their nanocomposites. These methods are Melt Blowing, Bicomponent Fiber spinning, Phase separation, Template Synthesis, Self Assembly, Electrospinning, Centrifugal spinning. In Melt blowing, the polymer is subjected to heat and is being made to melt.Then the melted polymer is extruded in form of jets through multiple nozzle at the same time using high velocity air streams and the fibers are collected randomly to form a non-woven fibers[41]

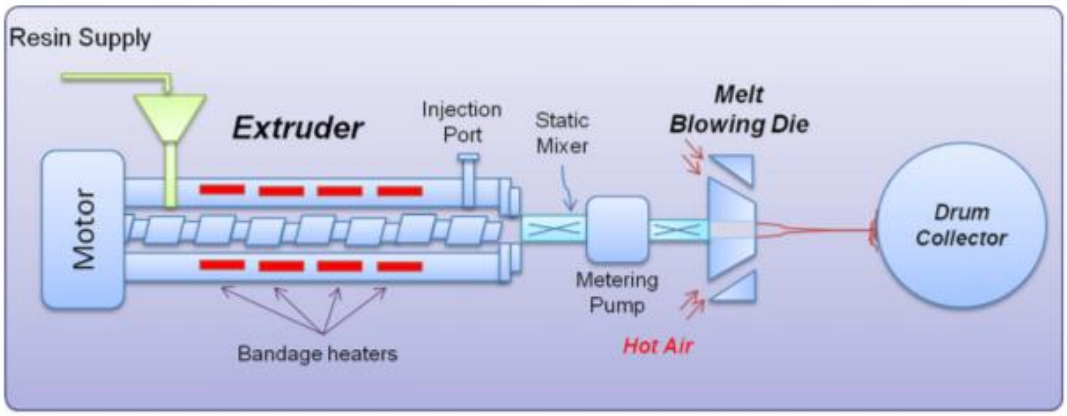

Figure 1. Schematic drawing of Melt Blowing process

This technique has been used to fabricate fibers from poly(butylene terephthalate) (PBT) [41] In addition to Melt Blowing method of fabricating fiber is Bicomponent Fiber Spinning in the nanofibers are produced by separating the different components that consist of two immiscible polymer. The islands-in-sea have multiple fibrils that consisted one of the polymer components. The bicomponent fibers formed are splitted so that one of the components is used to make nanofiber and this technique has been used to fabricate PET from PET/PE bicomponent due to the thermal differences between PET and PE[42].In addition to Melt Blowing is Template Synthesis method of fabricating nanofiber.In this method the nanofibers are fabricated in hollow channels of polymer or ceramic template. Firstly, the starting materials for the nanofiber fabrication are poured in the porous template. The nanofiber are fabricated after the starting materials, polymers, are dissolved or etched from the template. Also polymer solutions can used to produce nanofiber by feeding the solution into the template and the solution is allowed to form solid after the evaporation of the solvent. This method has been used to fabricate conducting polymer based nanofiber of polypyrrolidone in which the morphology of the PVP nanofiber has superhydrophobic property having contact angle above 165^0[43]. Furthermore, Self-Assembly is another non-famous method of fabricating nanofibers. This technique uses the intermolecular interaction to hold small molecules together. This fabrication method is used to produce hydrogel which involves two interpenetrated liquid phase and solid phase. The liquid phase is usually water and the solid phase is a network of nanofibers formed from the self-assembly. This method has been used to fabricate biomaterials such as protein nanotubes and helical ribbons, the fabrication of living micro lenses, the synthesis of metal nanowires on DNA

template, the fabrication of peptide and protein and lipid scaffolds[44] Another nanofiber fabrication method is Phase Separation ; this involves the polymer is first dissolve and form a homogenous solution at room temperature, the solution is then allowed to form gel at the room temperature and phase-separates to nanofibers after the solvent has been removed. This technique has been used to fabricate poly(L-lactic acid) (PLLA) nanofibers[45].The famous technique of fabricating nanofibers is Electrospinning. The set up for electrospinning consists of a syringe, a metal nozzle, a power supply and a collector. This method involves the use of high voltage being applied between a syringe containing spinning fluid and a metallic conductor. A critical value of the voltage, the fluid is electrically charged to generate a conical droplet, called Taylor cone, where a liquid jet is formed and allowed to stretch and whip to make the jet diameter to decrease from micrometers to nanometers and the stretch jet is collected on the surface of the grounded collector. The properties, such as the morphology and diameter, of the electrospun nanofiber depend on i) intrinsic properties of the polymer solution such as the viscosity of the solution, surface tension, conductivity of the solution, the molecular weight of the polymer

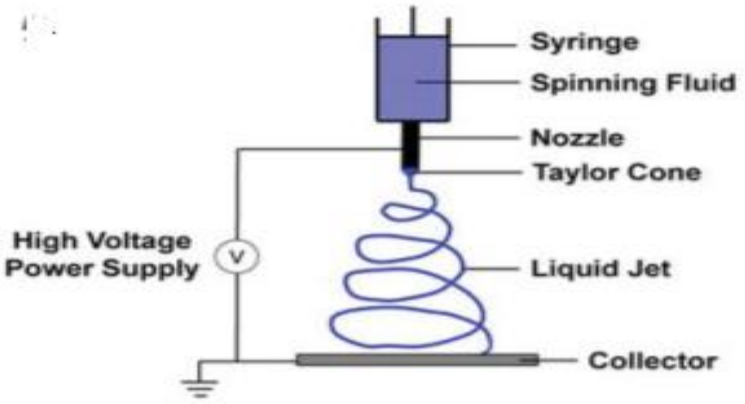

Figure 2. A schematic of a single-nozzle electrospinning system

the solution concentration, and ii) operational conditions of the electrospinning set up such as the electric field strength, solution flow rate, nozzle diameter, the collector distance from the nozzle, nozzle diameter. This process is highly tunable process because the diameter of the fiber can be tuned by adjusting the applied voltage, polymer solution concentration[46].This nanofibers fabrication method has been made to fabricate several nanofibers and nanocomposites. Electrospinning has been used to produce nanocomposite of polyamide-graphene-oxide polypyrrole in which the composite was used as a sorbent for spin-column micro solid phase extraction that used to determine the preservative, paraben, in milk samples[47]. Electrospinning has been used to fabricate poly(e-caprolactone) that is used in highly porous 3D nanofiber scaffold for tissue-engineering[48]. Polyurea nanofibers based on polypropylene oxide polyetheramine and isocycyanante has been electrospun for the purpose of analysis of the nanofibers mechanical properties under dynamic conditions[49].Electrospinning has been used to fabricate co-nanofibers of poly(ethylene oxide) (PEO) and poly(methyl methacrylate) (PMMA)

with good thermal stability[50]. Electrospinning has been combined with centrifugal field to fabricate nanofiber of polylactic acid (PLA) with high crystallinity, molecular orientation ,conformation and good mechanical stability[51]. Electrospinning has been used to fabricate coaxial nanofibers in which the fibers were integrated into water borne polyurethane coating for coatings self-healing[52].Highly aligned poly(vinyl alcohol) (PVA) nanofibers were fabricated by electrospinning for applications in the areas of filter media and microelectronics[53]. MgO nanocomposite was fabricated via electrospinning technique using polyvinyl alcohol/ magnesium precursor that is used in the photocatalytic degradation of industrial dye effluents[54]. Electrospinning has been used in fabrication of carbon nanofiber from the precursor of polyacrylonitrile (PAN)[55].

A new technique of fabricating nanofibers and their nanocomposites is called Forcespinning™ which uses centrifugal force to fabricate nanofibers and their nanocomposites from polymer solutions or polymer melts[12]. This technique is used to overcome the limitations of the other nanofibers fabrication techniques such as low production rate, the safety and environmental related issues , limited polymer materials that could be fabricated to nanofibers and cost effectiveness[17].The centrifugal force technique is made of system of rotating head which is coupled with spinneret and nanofiber collecting system. The spinneret is attached with two needles. At a critical speed of the rotating head, centrifugal force is generated that produces liquid jets at the same time from the attached needles. The centrifugal force causes the stretching of the liquid jets which allows the solvent to evaporate, and the jet is deposited on collectors in form of nanofibers.

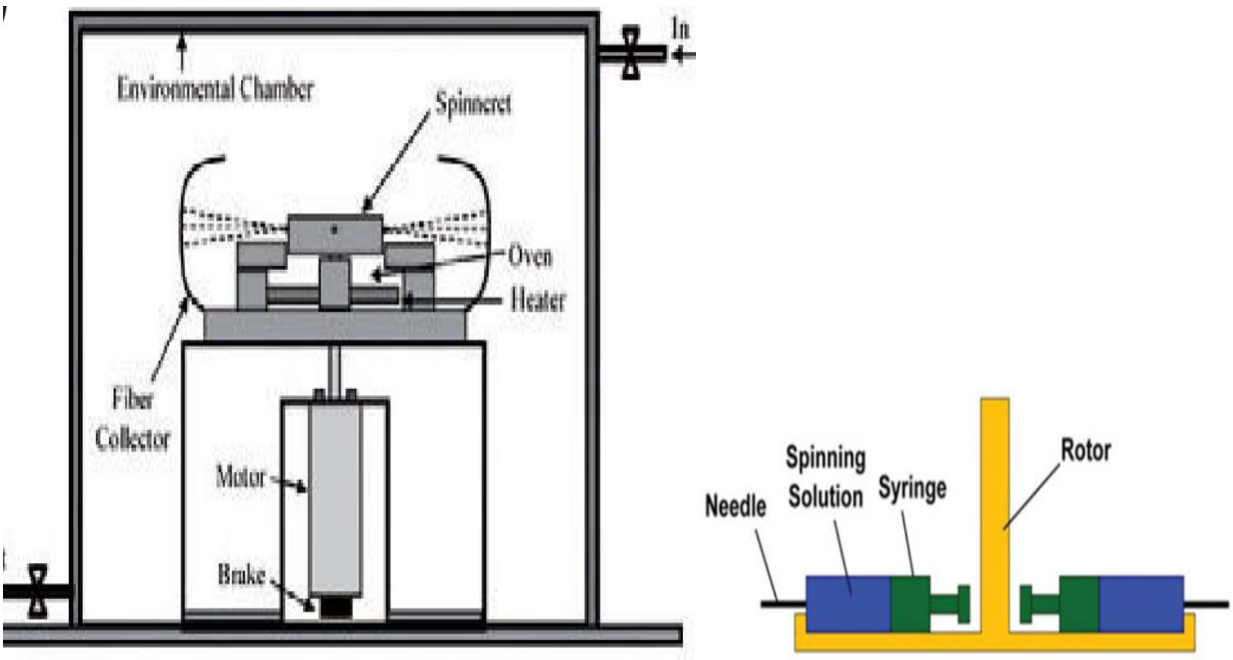

Figure 3 (a) A prototype Forcespinning™ machine[12] (b) A syringe-based spinning head [17]

The morphology of the nanofibers are dependent on processing parameters such as(i) intrinsic properties of the spinning fluid such as solution viscosity ,surface tension, molecular structure, molecular weight, solution concentration solvent structure and additives, and (ii) operational conditions of the forcespinning machine such as rotating speed , spinning head diameter, nozzle diameter and nozzle -collector distance[48],[56],50],[58]. This technique has been used to fabricate nanofibers and nanocomposites from different polymeric solutions and nanocomposite precursors. Centrifugal spinning (CS) has been used to fabricate porous carbon nanofibers as

binder-free electrode for electric double layer capacitors from precursor of polyacrylonitrile (PAN) /poly(methyl methacrylate (PMMA) after the nanofiber were subjected to thermal treatment[59].Centrifugal spinning has been used to fabricate PA6 nanofibers to study the solutions properties and also the morphology of the spun nanofibers. Forcespinning has been used to fabricate lignin-thermoplastic polyurethane polymer blends[60].Centrifugal spinning has been used to fabricate poly(acrylic acid) nanofibers[16]. Polyvinyl alcohol was centrifugally spun as precursor to study the mechanical and electrical characterization of carbon nanofibers[61].Polyvinylpyrrolidone solution has been centrifugally spun to form nanofibers for the purpose of elucidating the processability and characterization of this nanofibers[62]. Thermoplastic polyurethane (TPU) was centrifugally spun for air filtration application[63]. Fabrication of nanofibers of PA6 was done using centrifugal force for the purpose studying the occurrence and morphology of bead-on-string structures[64].Polyacrylonitrile(PAN) nanofibers were fabricated through centrifugal spinning of PAN solutions to establish spinning parameters to have better nanofiber morphology[65].

Characterization of Polymer Nanofibers Using Spectroscopic and Thermal Methods

The morphologies of polymer based nanofibers has been studied using scanning electron microscopy (SEM).The SEM images has been used to reveal the topography and morphologies of several polymer based nanofibers. Some of the polymer based nanofibers that their morphologies have been reveal are PVP[66], PAN[67],Polyamide 6 (PA6)[68], PEO[58],Polyvinyl alcohol(PVA)[69], Poly(acrylic acid) (PAA)[16], PET[70],Polyurea[49], Polylactic acid(PLA)[51].

Fourier Transform Infrared (FT-IR) spectroscopy has been used to provide information about the functional group in fabricated polymer-based nanofibers. PEO FT-IR spectra has shown major peaks at 2884cm^{-1}, 1468cm^{-1}, 1146cm^{-1} which corresponds to C-H stretching band, scissoring mode and C-O-C stretching vibration[50]. The FT-IR spectra of poly (methyl methacrylate) show peaks at 2950cm^{-1} and 1730cm^{-1} which connotes the C-H stretching band and C=O stretching band[50].

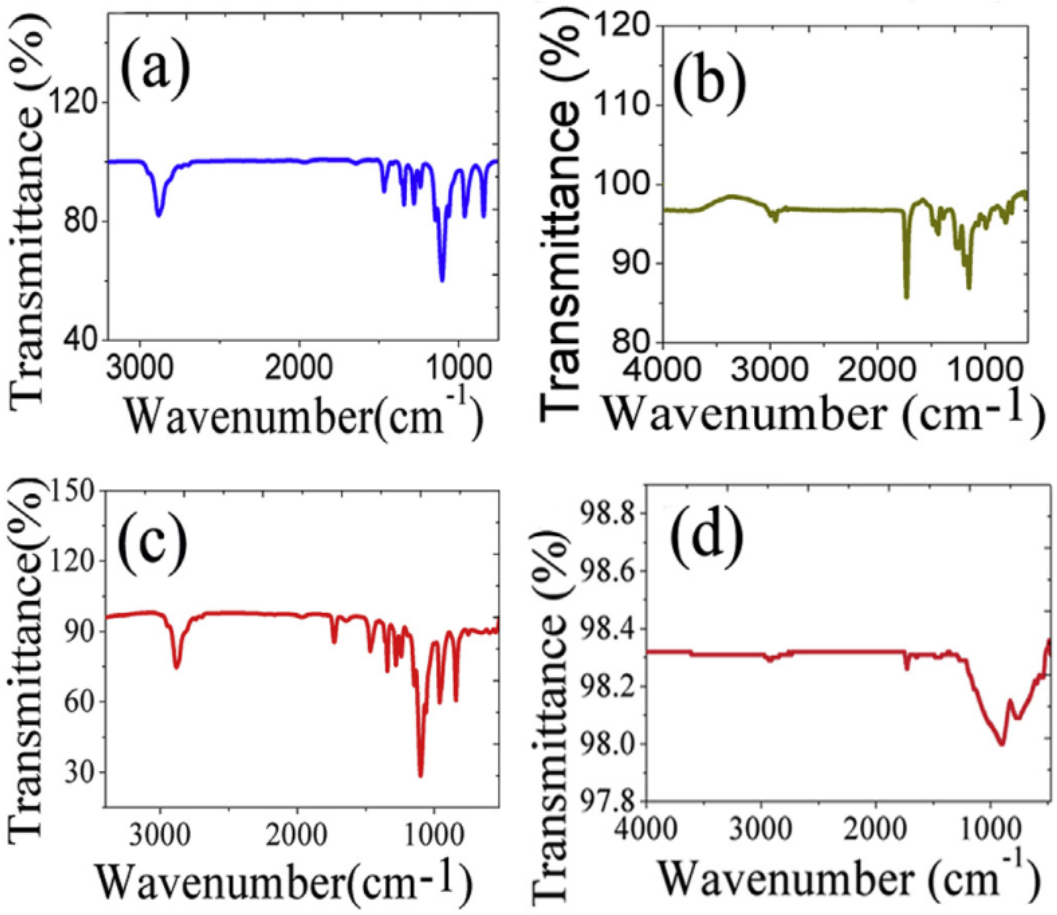

[50]

Figure 4 .FTIR spectra (a) Pure PEO (b) Pure PMMA (c) PEO-PMMA blend (d) Surface roughed PMMA

Silica fibers were validated by FT-IR spectra with characteristic peaks at 800cm^{-1}, 1123cm^{-1}, 1220cm^{-1} which are due to Si-O bond[71]

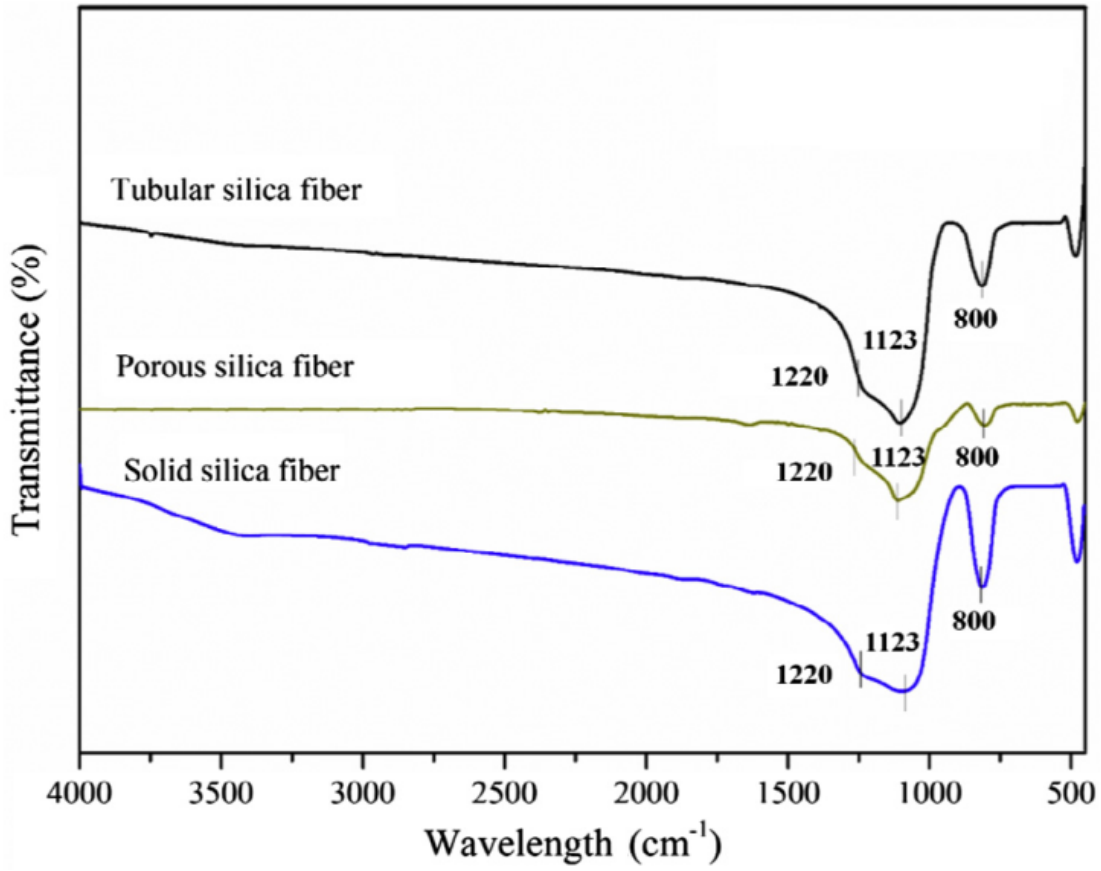

[71]

Figure 5. FTIR spectra : silica fiber with tubular structure ,porous structure and solid structure

.FT-IR has been used to determine the composition of nanofibers in which polyamide(PA) show absorption peaks at 1660cm^{-1} and 1539cm^{-1} which belong to C=O stretching vibrations and the N-H deformation vibration. Also graphene oxide (GO) show absorption peaks at 3200cm^{-1}. Polypyrrole show peaks at 1547cm^{-1}. This peak is due to C-C and C=C stretching vibration in polypyrrole[47]

.The ATR spectrum of co-nano fibers of PAN-PVA at 3328.9cm-1 and 1092.9cm-1 could be attributed to stretching vibrations of hydroxyl group(OH) and C=O respectively[72]

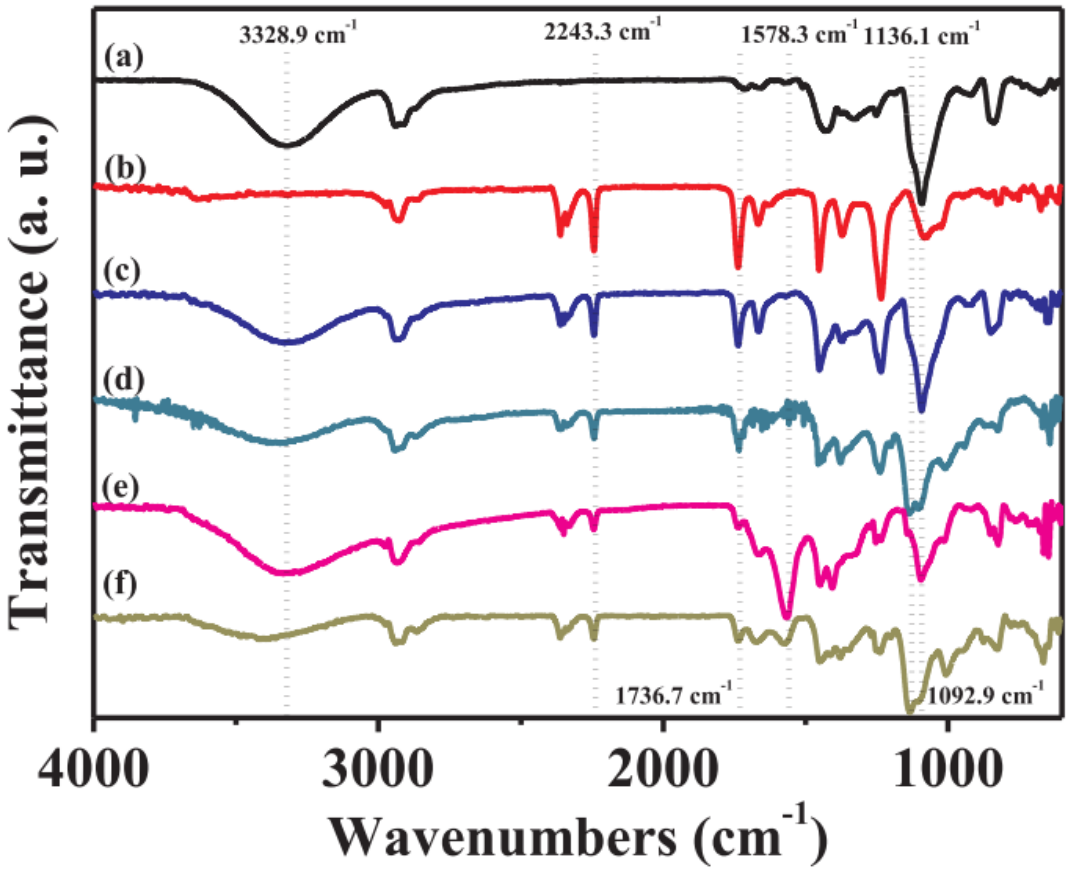

[72]

Figure 6.ATR spectra of (a) PVA membrane, (b) PAN membrane, (c) PAN-PVA

FT-IR spectra of polyethylene glycol and polyethylene oxide absorption bands have been due to C-O ,C-C stretching ,CH_2 rocking at 840cm^{-1}, CH_2 rocking, CH_2 twisting at 960cm^{-1}, C-O, C-C stretching ,CH_2 rocking at 1058cm^{-1}, C-O, C-C stretching at 1097cm^{-1}, C-O stretching. CH2 rocking at 1145cm^{-1}, CH_2 twisting at 1241cm^{-1} and 1278cm^{-1}, CH_2 wagging at 1341cm^{-1} and CH2 scissoring at 1466cm^{-1} [73].FT-IR has been used to analyze blends of Polyvinyl pyrrole(PVP) and polystyrene (PS). The PS show absorption bands at 2922$cm^{-1}$are due to

asymmetric stretching vibrational modes of the CH2 group also absorption bands at 1600cm^{-1} is attributed to C-C stretching mode of the phenyl group. For PVP, there are characteristic absorption peaks at 1658cm^{-1} and 1288cm^{-1} which are due to C=O and C-N vibrations[74]. The confirmation of the blending of PAN/PMMA polymer - based nanofiber was done using FT-IR. The absorption band at 2220cm^{-1} is due to the C ≡ N stretching of PAN. The band at 1730cm^{-1},1239cm^{-1} and 1149cm^{-1} are from C=O, C-O, C-O-C stretching respectively from PMMA. The blend was successfully prepared because both PAN/PMMA showed the characteristic bands of PAN and PMMA[75].

Raman Spectroscopy provides information on the structure (composition, stress/strain state, crystal symmetry and orientation, quality of the crystal of nanofibers. Raman spectroscopy has been used to study crystallinity in polymers[76]. Raman spectroscopy has been used to investigate bulk polyacrylic acid (PAA) and nanofibers with line located at 508cm^{-1} this is due to bending motion of C-C=O groups. The bands between 613 and 645cm-1 to bending vibrations of trans C=O units. The symmetric vibrations in C-C=O and CH2 vibrations is due to 840cm^{-1}[16]. Crystalline and semi crystalline domains were observed in polylactic acid

Thermal analysis is used for the understanding and evaluating the structure and properties of polymeric nanofibers. Also thermal analysis are important factor to be considered in the processing ,application and storage of polymeric materials[16] Thermogravimetric Analysis (TGA) and Scanning differential calorimetry (DSC) are the most used tools in thermal analysis of polymeric materials. TGA and DSC have been used for the evaluation of glass transition

temperature(Tg), melting point temperature™ and heat flow, thermal breakdown, thermal stability ,weight loss in each stage of polymeric materials[77].

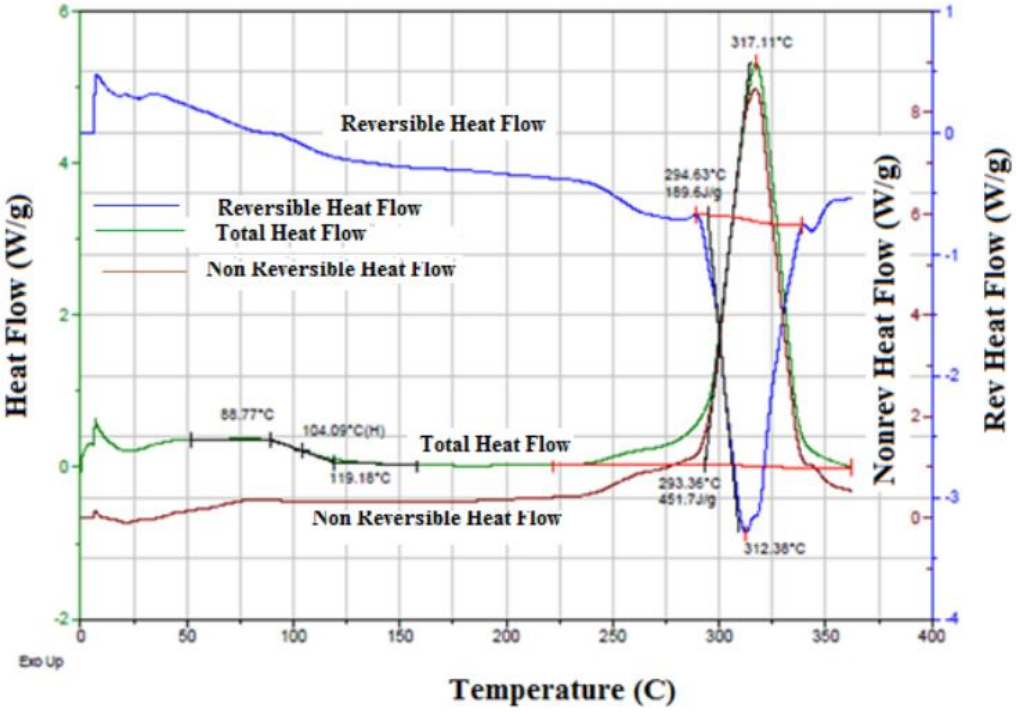

Figure 7(a). DSC thermograms of pure PAN fibers[77]

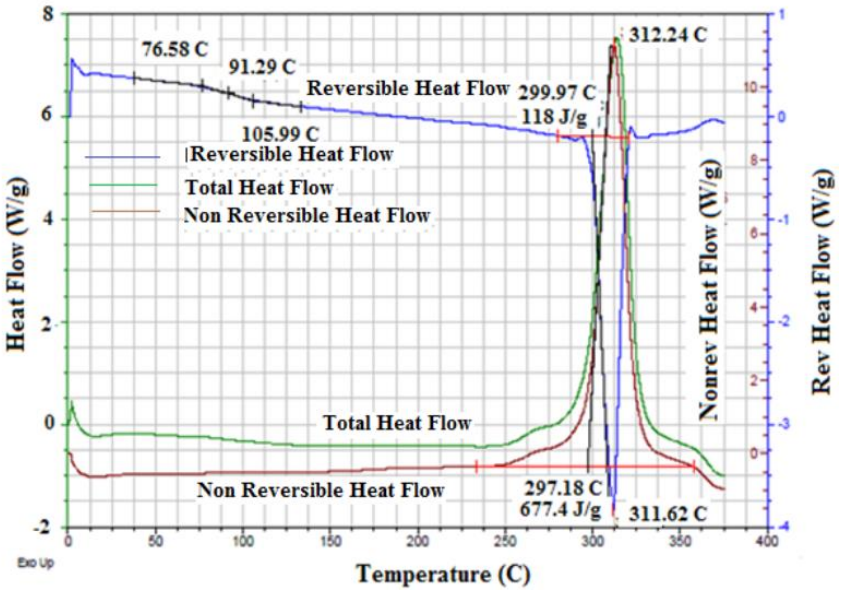

Figure 7(b) .DSC thermograms of bulk PAN [77]

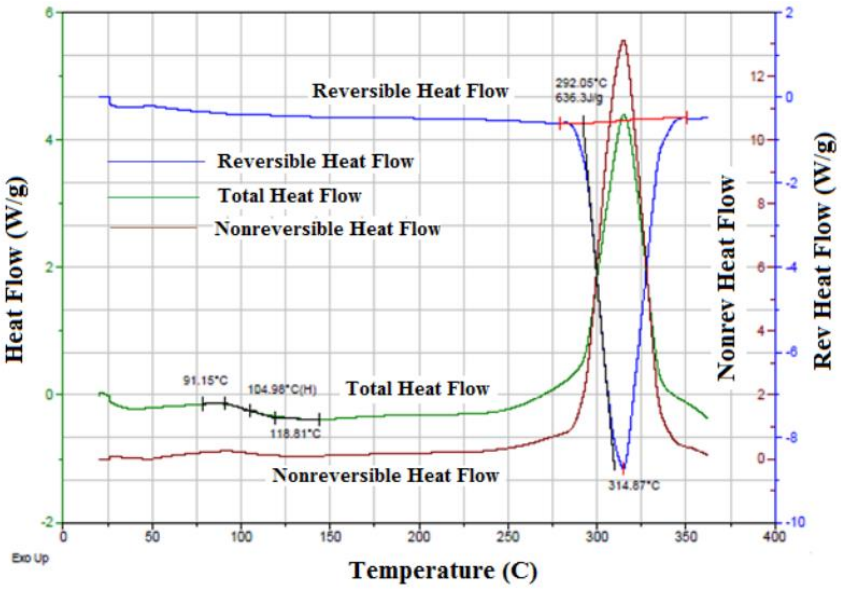

Figure 8. DSC thermograms of PAN nanocomposite fibers with 8 wt. % MWCNTs[77]

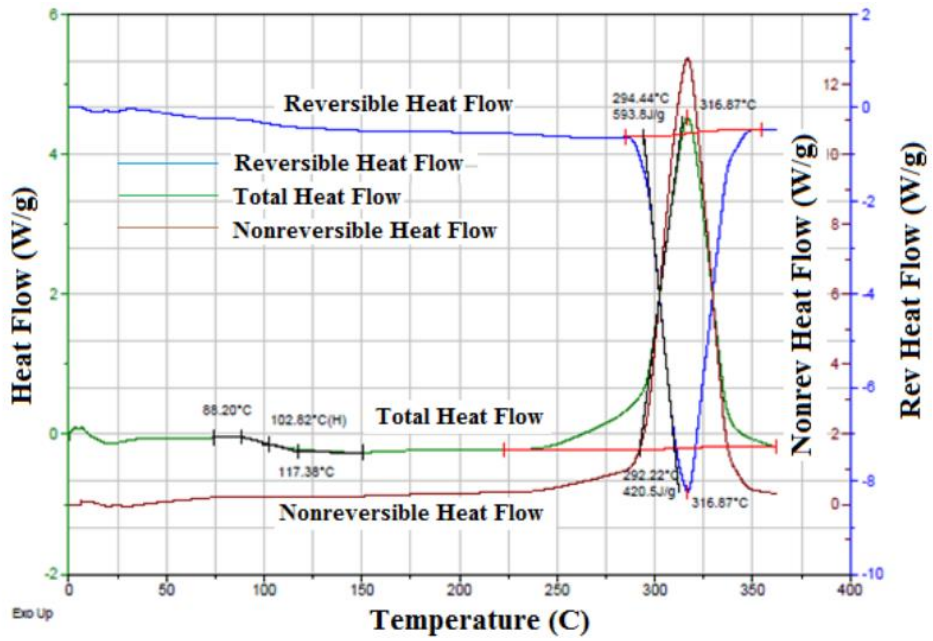

Figure 9.DSC thermograms of PAN nanocomposite fibers with 8 wt. % graphene nanoplatelets[77]

It was demonstrated by the DSC thermogram that addition of graphene to PAN fibers increased the glass transition. Also the degradation of the pure PAN and functionalized PAN, the fiber showed four-step weight loss[77]. TGA thermogram indicated that there are chemical reactions as the PAN heated which resulted in four-step weight loss and also the increase in the addition of graphene also increased the weight loss temperature[77].

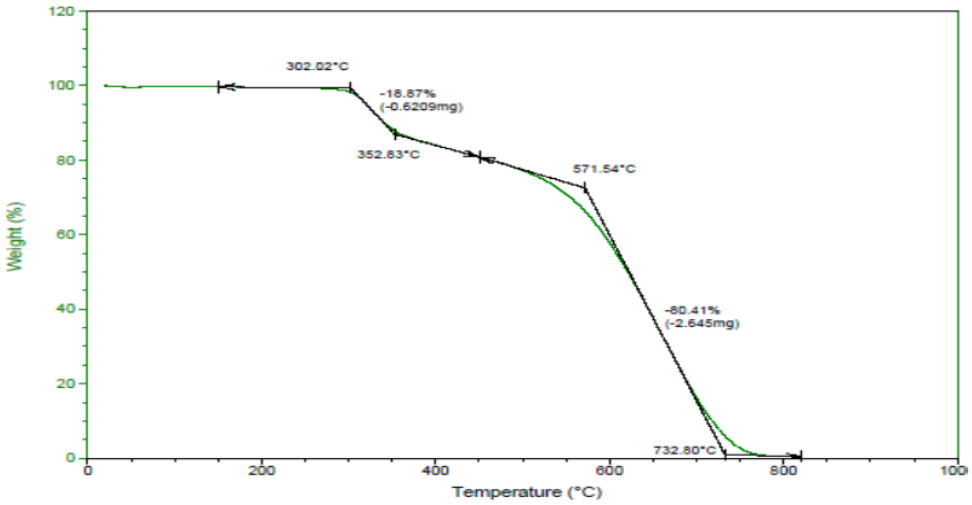

Figure 10. (a) TGA curve of pure PAN bulk

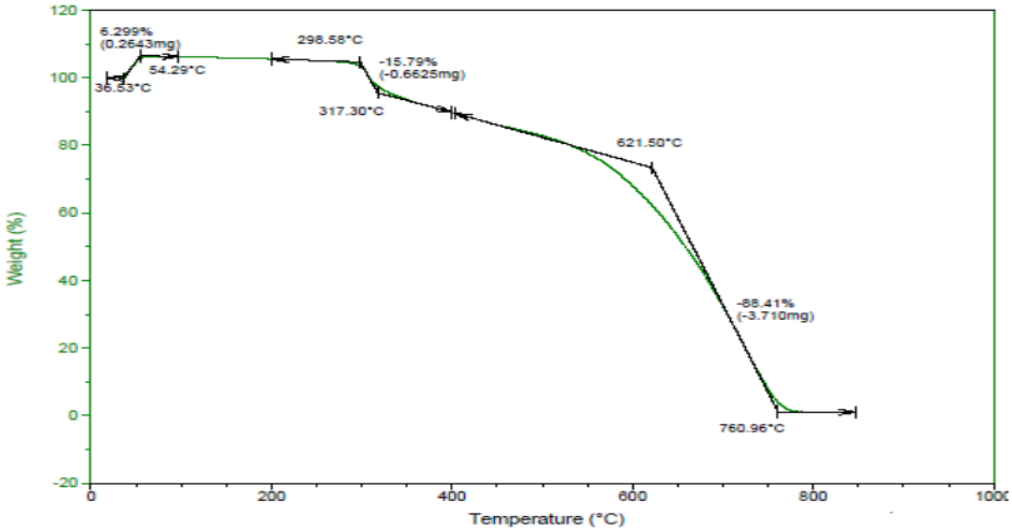

Figure (b)

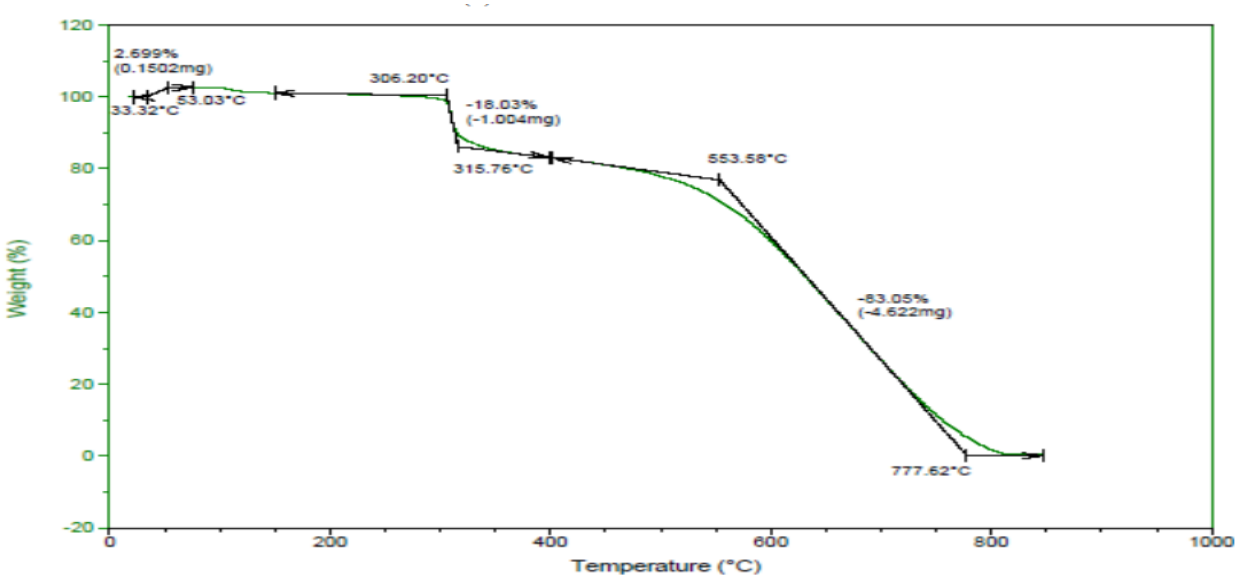

(c) TGA curves of PAN: (a) with 2 wt. % graphene, and (b) with 8 wt. % graphene[77]

Thermal properties of electrospun crosslinked PVA was studied using TGA and DSC, it was observed that there was decrease in melting temperature of the PVA polymer with crosslinking agent as shown by the DSC. Also the weight loss of the cross linked PVA happened at lower temperature of 240^0C than the weight loss temperature that occurred in the pure PVA at 290^0C[78]. Polypropylene nanofibers fabricated by forcespinning of the melt was analyzed using

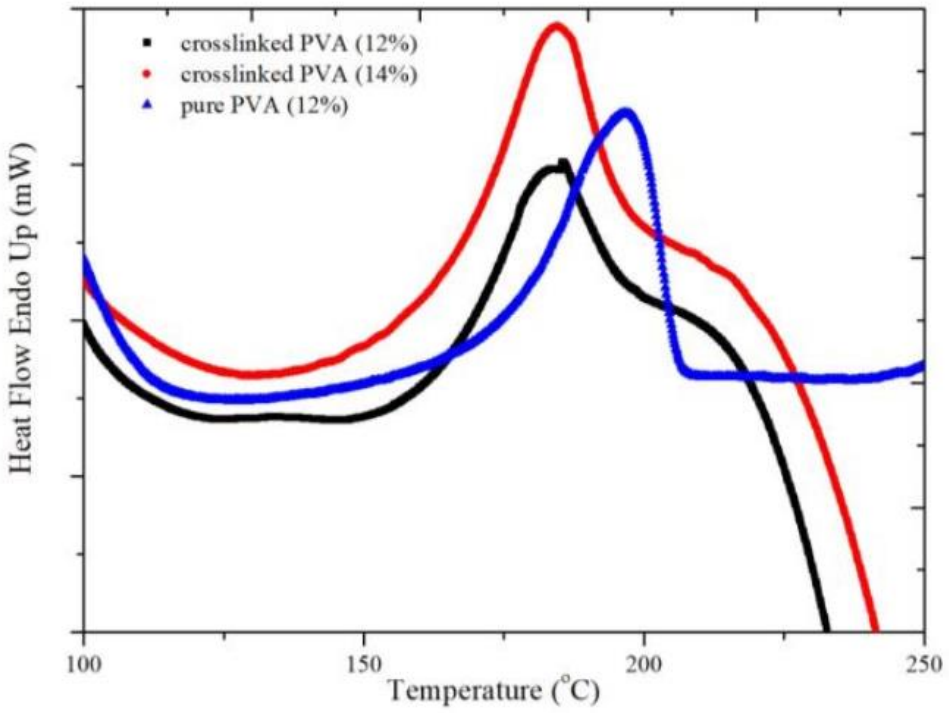

Figure 11 DSC graphs of crosslinked PVA (12%), crosslinked PVA (14%), and pure PVA (12%)[78]

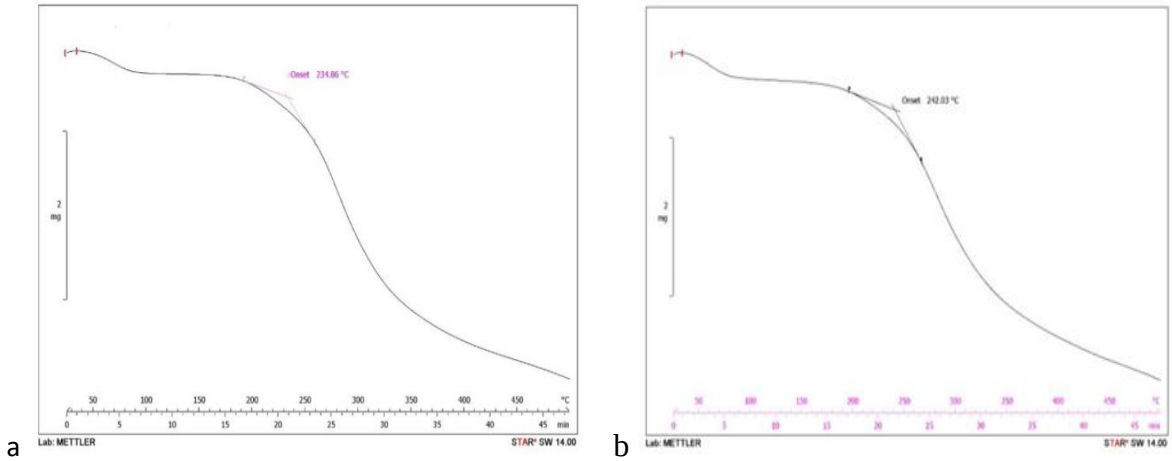

a b

Figure 12(a) TGA graph of crosslinked PVA (12%) (b) TGA graph of crosslinked PVA (14%) [78]

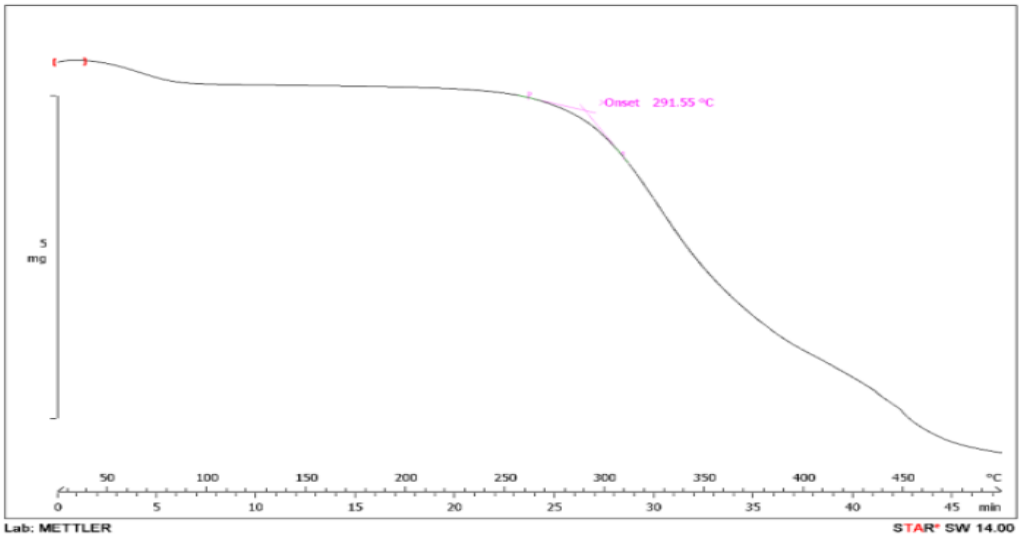

(c) TGA graph of pure PVA (12%)[78]

thermogravimetric analysis, it was observed that the forcespinning process had no effect on the thermal stability of the nanofibers[79]. Vapor grown carbon-nanofibers (VGCNFs) reinforced polyethylene nanofiber showed increase in thermal stability against the PE matrix as PE started degrading lower temperature[80] as shown below

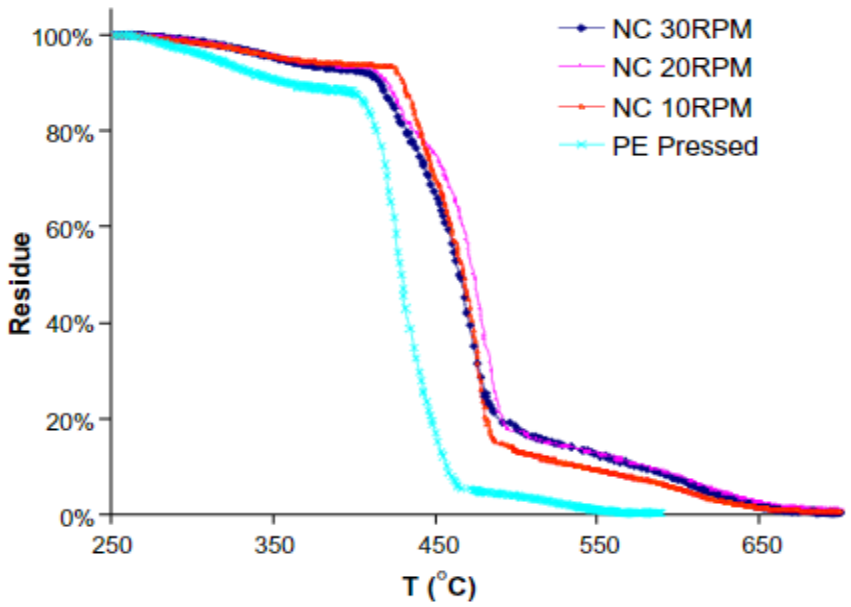

Figure 13 TGA curves of VGCNF-reinforced PE composites under Nitrogen[80]

An obtained thermogram from TGA of poly acrylic acid(PAA) with heating rate of 10^0C/min from 25^0C to 800^0C showed a total mass loss of 90% which was divided into three steps, mass loss due to evaporation of absorbed water ,formation of anhydride groups and the third

degradation was full degradation that remained 10% of carbonaceous residue[16].

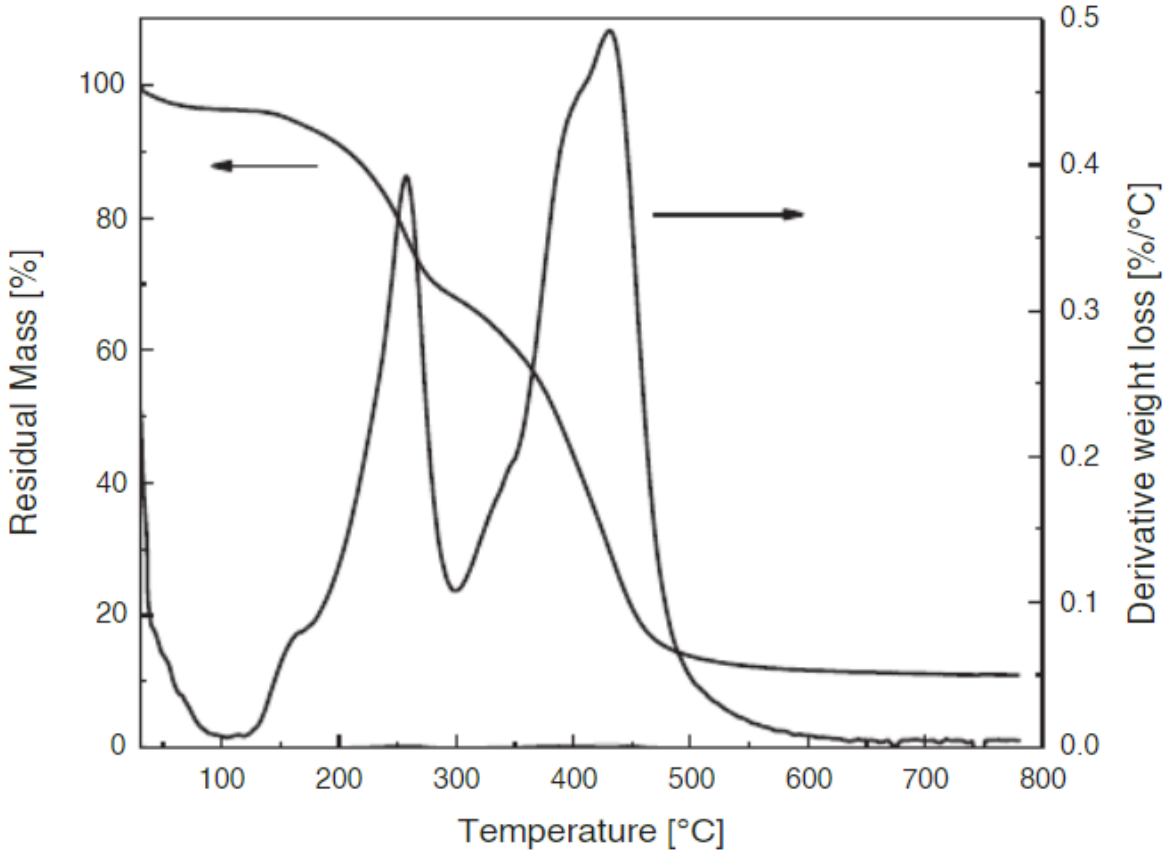

Figure 14 TGA and derivative thermogravimetric curves of PAA fibers [16]

The DSC spectrum showed a sigmoldal dependence of heat flow versus temperature where the glass-transistion temperature was at the middle of the dependence[16] as shown in figure

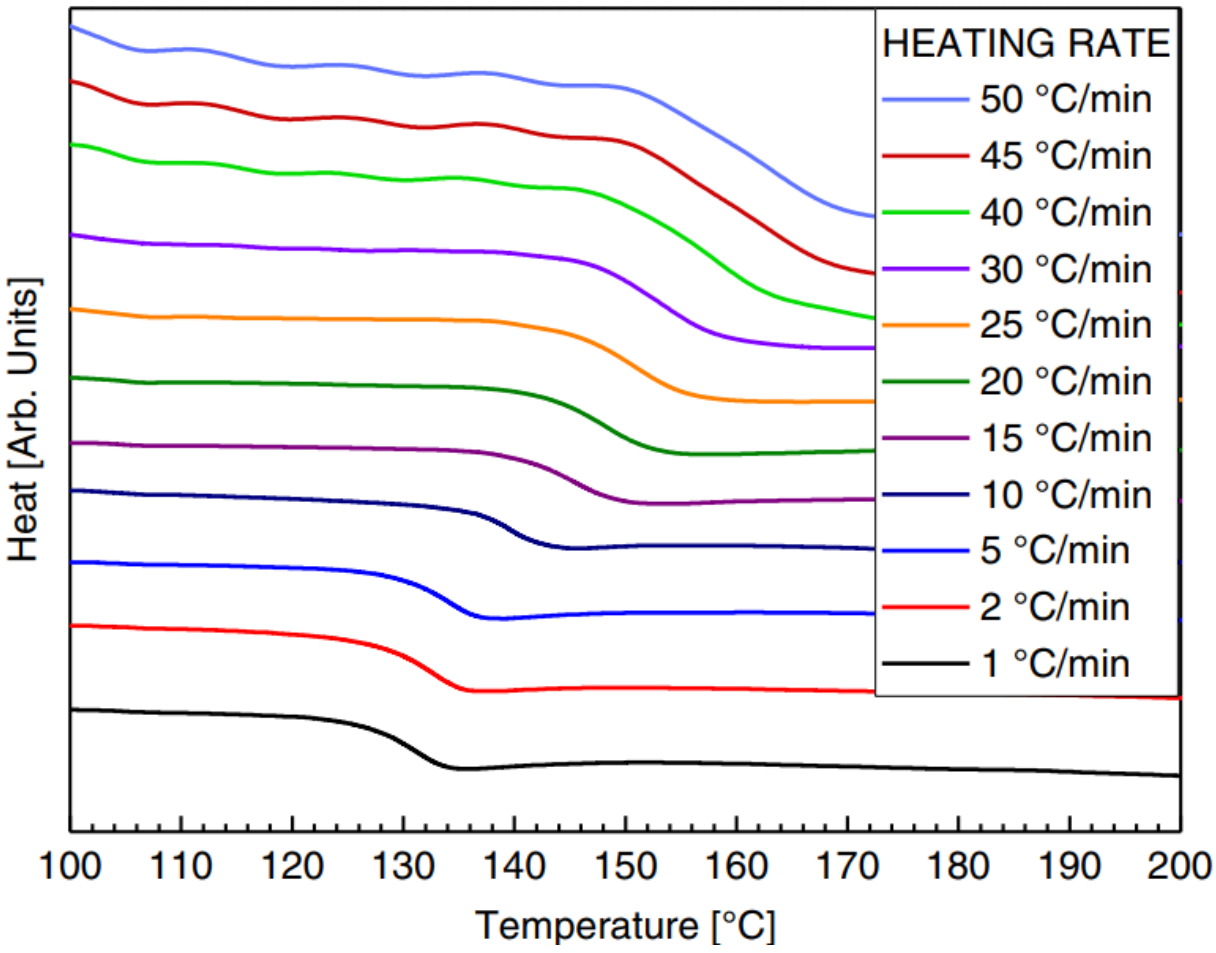

Figure 15 DSC spectra of PAA bulk at different heating rates [16]

Thermal properties of polypropylene (PP) polymer and melt blown fibers were compared. The DSC thermograms showed that PP and the fibers indicated melting point of 165.5^{0}C;but the fibers from injection of fluids showed melting point of 152.5^{0}C-155.5^{0}C which indicated in crystalline phase[81]. Also cold crystallization were observed in both polymer as-spun fibers at 113.5^{0}C and 110.5^{0}C but the cold crystallization for the fluid fabricated fibers was at 107.5^{0}C.The lower values of the fluid fabricated was due to the degradation caused by the heat pre-treatment of the injection fluids as this was proved by the TGA[81]

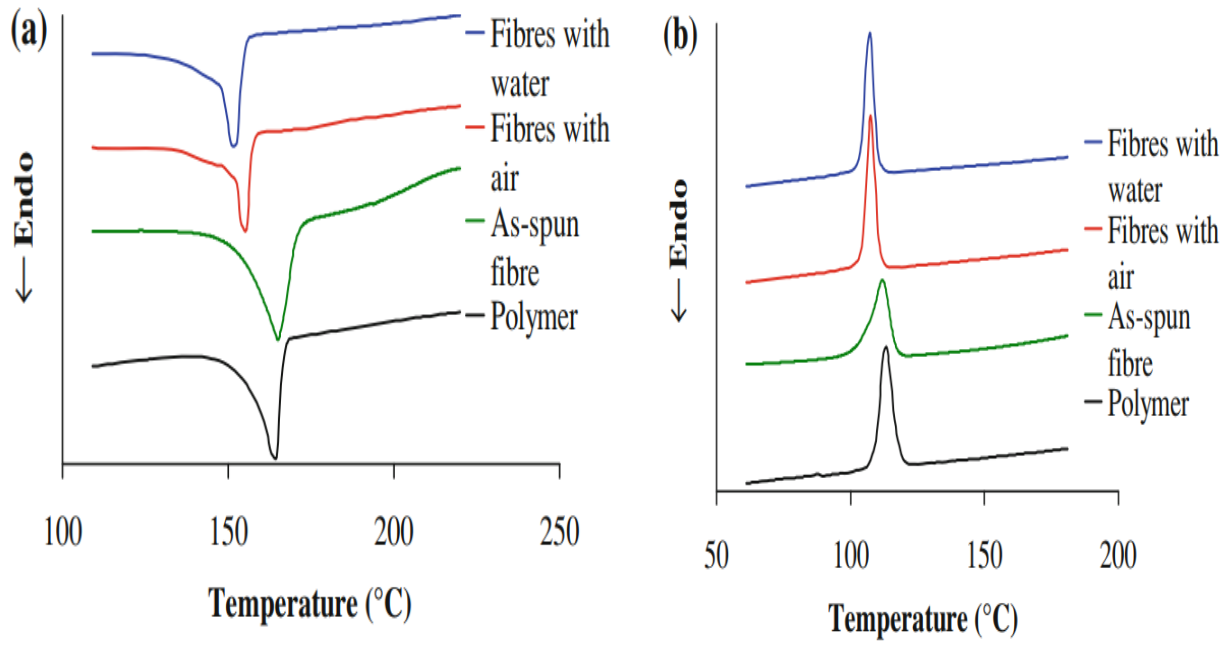

Figure 16 The DSC curves of melt blowing PP polymer and fibers of meltfluid injection of first (a) and second heating (b)[81]

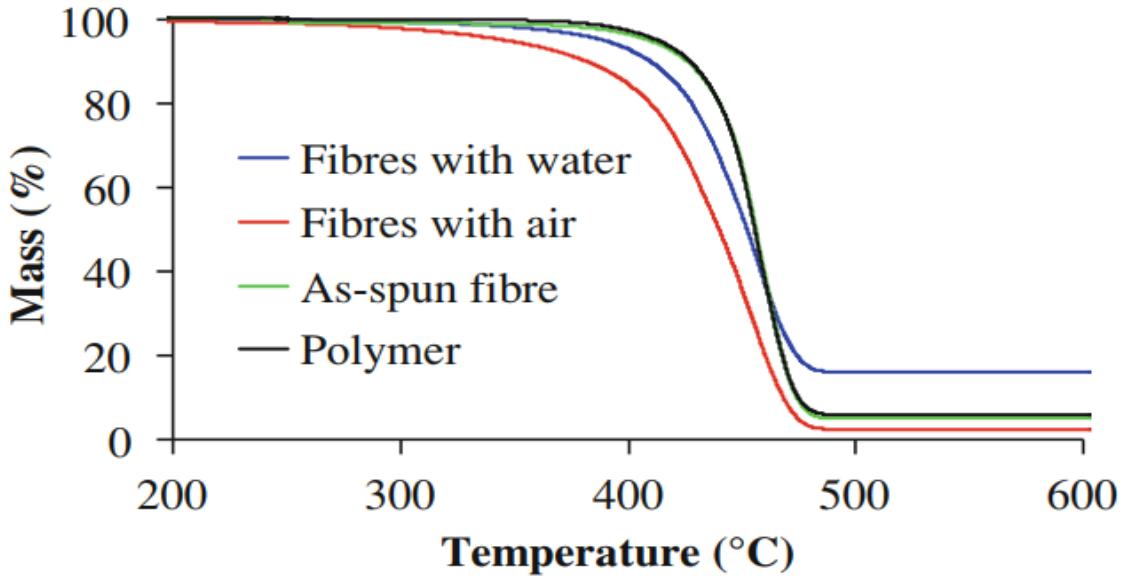

Figure 17 The TGA thermogram of PP polymer and meltblown fibers from 300 Meltfluid injection [81]

Thermal analysis was used to reveal the blend of lignin -thermoplastic polyurethane (TPU) fabricated nanofiber and neat TPU by DSC, it was showed that both the co-nanofiber and the neat TPU have both similar thermal behavior. The showed a plateau of 130^0C and a peak of 204^0C which were the softing and melting temperature while the co-nanofiber of lignin and thermoplastic urethane have endothermic peak at 187^0C and slope at 140^0C displaying the lower melting point and higher softening temperature due to the presence of lignin in the blend[60]

...

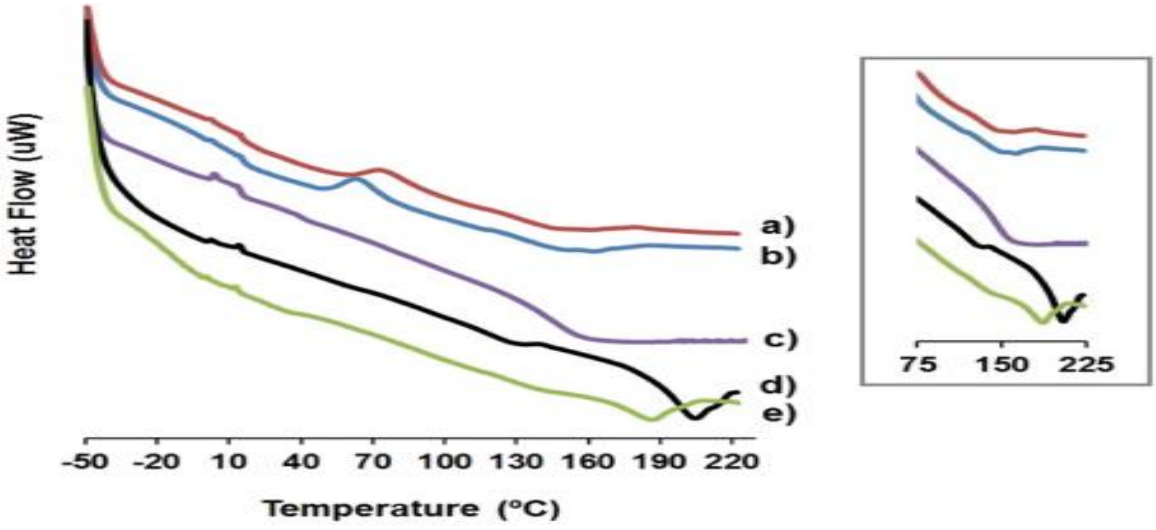

Figure 18 DSC analysis of (a) 1:1, (b) 2:1 (blue) lignin/TPU nanofiber (c) lignin powder (violet) ,(d) TPU

granules (black) and (e) 1:2 (green) lignin/TPU nanofibers [60]

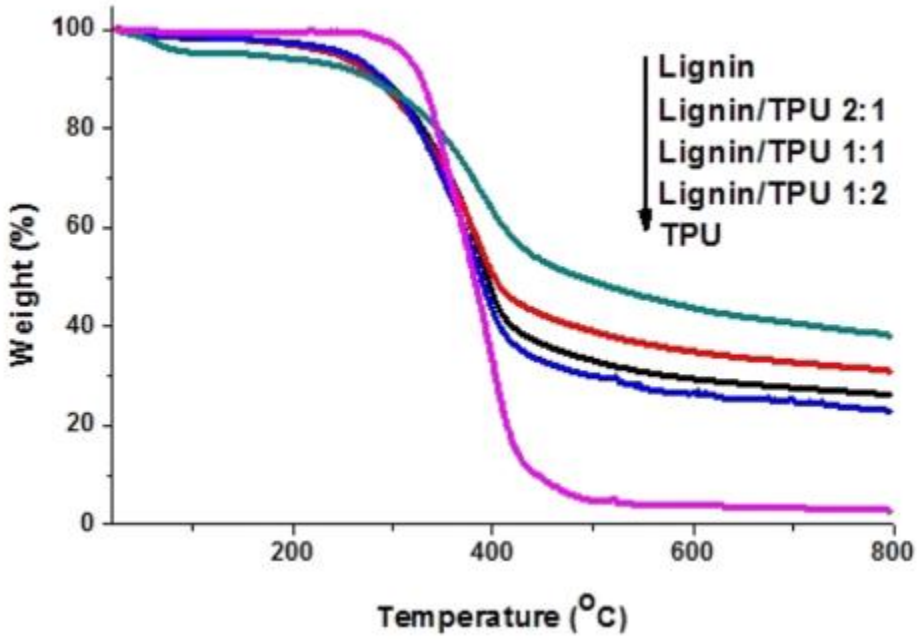

Figure 19 Thermogravimetric analysis of lignin/TPU nanofibers, lignin powder and TPU granules[60]

The TGA showed that the neat TPU degraded in two steps with the first step at 260^0C because of the hard segments and the second complete degradation step was around 440^0C but the neat lignin started degrading at 50^0C due to evaporation. The removal of side chain caused the degradation to be between 250-450^0C [60].

CHAPTER III

METHODOLOGY AND FINDINGS

Experimental Details

Materials

Polyethylene oxide (PEO) of average molecular weight 9x 10^5 g.mol^{-1} and 1x 10^5 g.mol $^{-1}$were purchased from Aldrich and used as it is. De-ionised water was obtained from --- and also used as obtained. Poly(vinylpyrrolidone),(PVP) of average molecular weight 1.3X 106 was purchased from Acros Organics and used as it is.

Preparation of Polymer solutions

The PEO powder was dissolved in water to produce different concentrations of 6%(w/w), 8%(w/w) and 10%(w/w) at 60^0C using magnetic stirrer to aid in the dissolution of the polymer. PVP solutions of different concentrations were made (12%, 16%,18%, 20%, 24% and 26%(w/w)) by dissolving the PVP in water and mechanically stirred with magnetic stirrer. Co-copolymer solutions were also made by blending PEO and PVP ranging from PEO: PVP 50% :50%, 75% :25%, 25%: 75%. Polymer nanocomposite solutions were also made by introducing different percentages of C60(from 0.5(w/w) through 20%(w/w) in PEO solutions

Nanofiber Precursor Solutions Analysis

Surface Tension

The surface tension of the solutions was determined using FAMAS interface measurement and analysis system (KYOWA interface science Co. Japan)

Solution Viscosity

The viscosities of the solutions were evaluated at 220C using Brookfield DV-111 Ultra Rheometer coupled with spindle numbers 02,03,04,05,06 and 07. The spindle number 07 was adopted for this exercise because it gave viscosity readings for all the samples.

Nanofibers Fabrication

The PEO solution was fed in spinneret of Forcespinning machineTM that was coupled with needle size 30G and with eight standing collectors at 15cm from the spinneret and the rotational speed was set between 6000 RPM and 10 000 RPM. The formed nanofibers were collected from the aluminum standing collectors.

Characterization of the PEO and PVP nanofibers

Scanning Electron Microscopy

The nanofibers, n were subjected to Scanning Electron Microscopy (SEM; Sigma VP Carl Zeiss, Germany) for morphological and diameter measurement. The nanofibers were placed on the with the aid of carbon tape. The nanofibers were sputtered for 90 seconds before been subjected to SEM measurement.The SEM analysis were analyzed at an accelerating voltage of 1.0 kV and magnification of 5.0K

Thermogravimetry Analysis

10 -12mg of the nanofibers were weight into ceramic crucible and carefully put into the NETZCH TG 209F3 that was laced with purge nitrogen and protective gas at flow rate of 20ml/min. Different heating rates of 1^0C/min, 5^0C/min, 10^0C/min, 20^0C/min, 40^0C/min, 50^0C/min were used. The heating was from 50^0C to 1000^0C with cooling rate of 10^0C/min.

Differential Scanning Calorimetry Measurement

The DSC (DSC 214 Polyma NETZSCH, Germany) machine was coupled with Nitrogen cooling system. A closed lid Al2O3 crucible was used as the compartment for the samples. The DSC measurement was carried out using different cooling and heating rates with the cooling set at -----70^0C and heating to 225^0C isothermally at 5 minutes for each of the heating and cooling rates.

Fourier Transform InfraRed Analysis

The FTIR used was Bruker Vertex 70 with accessory of A225/Q platinum ATR, multiple crystals CRY Diamond. The scanning was done at scanning rate 16 with resolution time of 2 cm-1, in the range of 4000cm-1 to 400cm-1 wavenumbers using ATR spectrum.

Image Processing

ImageJ software was used for fiber diameter measurement and the information was used in processing the statistical fiber diameter distribution.

Results and Discussions

The polymer solution concentrations that gave good yield of nanofiber were measured as function of viscosity in Centi poise . There is linear relationship between the polymer concentrations and the viscosity as shown in the figure 20(a)

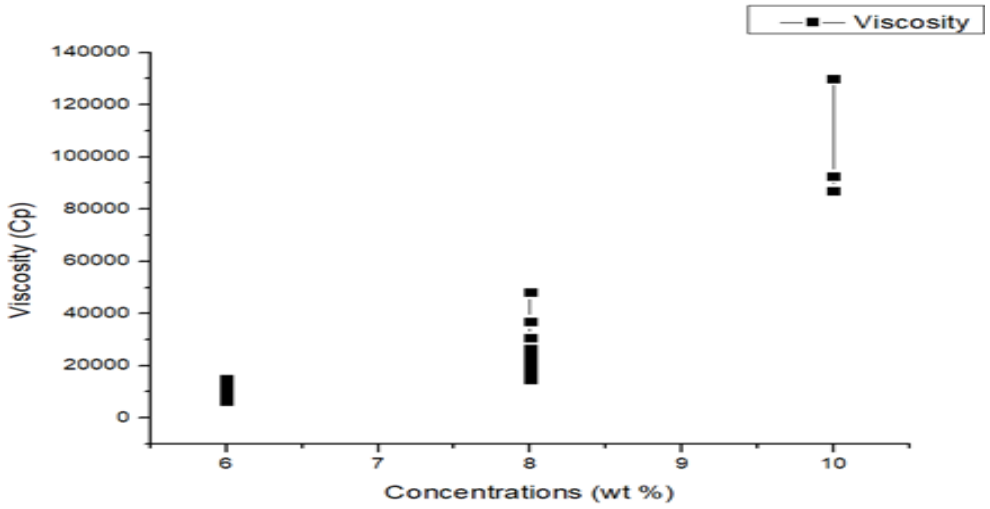

Figure 20 (a) A plot of viscosity as a function of concentration

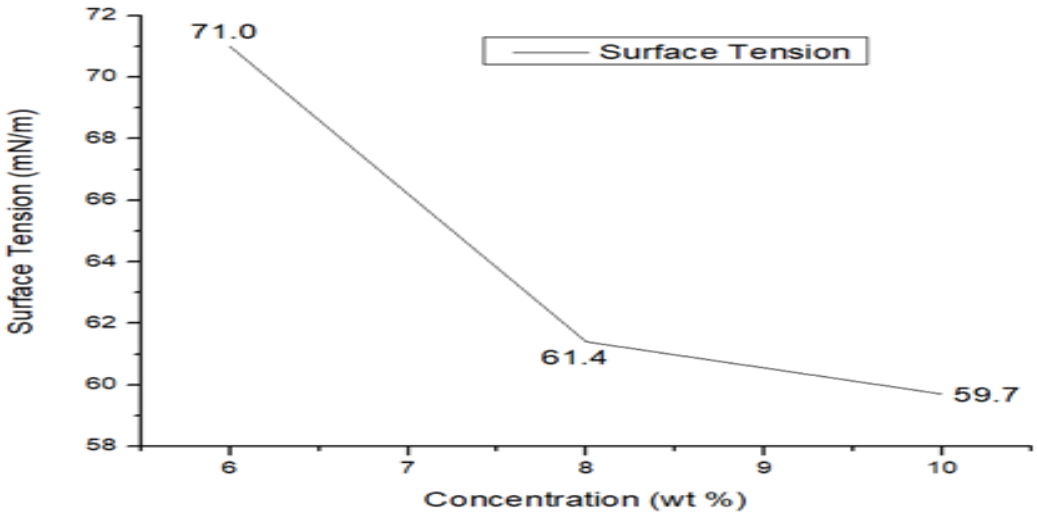

Figure 20 (b) A plot of PEO surface tension as a function of concentration

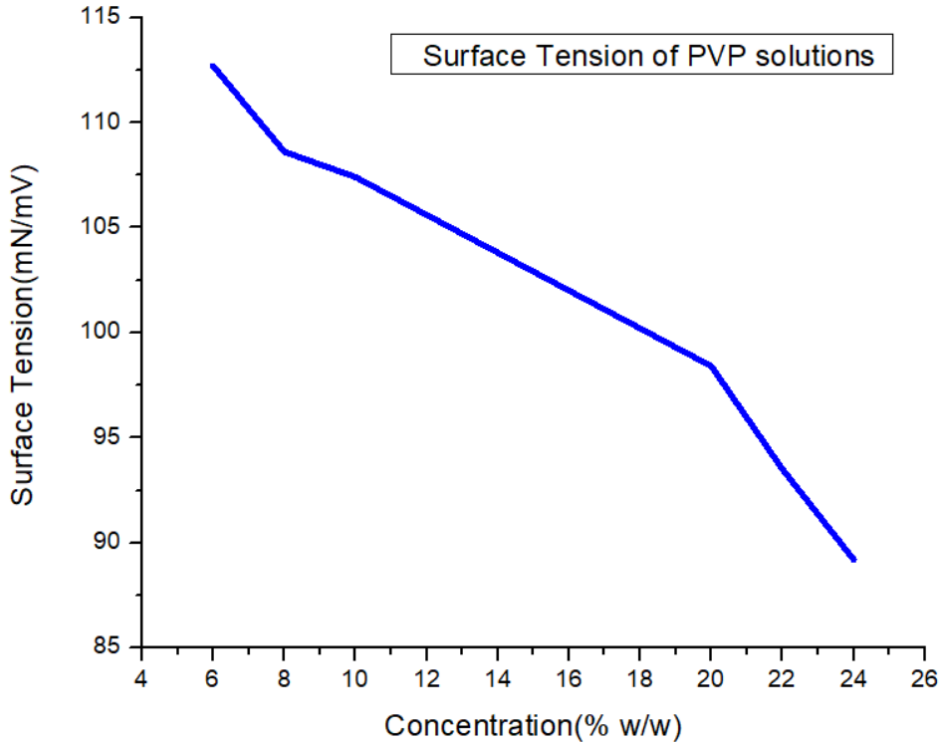

Figure 20 C .Plot of PVP surface tension as a function of concentration

Figure 20 (a) specific viscosity as a function of polymer concentrations. (b) Surface tension of PEO solutions as a function of concentrations (c) Plot of PVP surface tension as a function of concentration

Yield of Fabricated Nanofibers from PEO of Mw 900,000 in water

Solution Concentrations % (w/w)					Speed(RPM)	Duration(mins)
10	8	6	4	3		
V	P	P	P	P	10,000	5
V	P	P	P	P	9,000	5
V	G	P	P	P	8,000	5
V	V	P	P	P	7,000	5
G	V	V	P	P	6,000	5
P	V	V	P	P	5,000	5
P	P	G	G	P	4,000	5
P	P	P	V	P	3,000	5

* V: Very Good, *G: Good, *P: Poor

(a.)

Table 1 (a)

Yield of Fabricated Nanofibers from PEO of Mw 100,000 in water

Solution Concentrations % (w/w)					Speed(RPM)	Duration(mins)
10	8	6	4	3		
P	P	P	P	P	10,000	5
P	P	P	P	P	9,000	5
P	P	P	P	P	8,000	5
P	P	P	P	P	7,000	5
P	P	P	P	P	6,000	5
P	P	P	P	P	5,000	5
P	P	P	P	P	4,000	5
P	P	P	P	P	3,000	5

(b.)

Table 1(b)

Table 1 (a) PEO Mw 900,000 $g.mol^{-1}$ with different solutions concentrations and different spinneret speed rates

(b) PEO Mw 100,000 $g.mol^{-1}$ with different solutions concentrations and spinneret speed rates

Also the surface tension of the solutions and the concentrations as analyzed by FAMAS interface measurement and analysis system are inversely related [23] as shown in figure 20(b)

From the SEM images in figure 21(a-d) , showed the morphology of the nanofiber observed was cylindrical . This confirms that PEO cylindrical morphology has volume that can promote cell adhesion and growth that can also accommodate bioactive in its structure for drug delivery[24]. The nanofiber of PEO 8wt% solution spun at 7000 RPM has fiber diameter in the range of 2µm to 16µm while the nanofiber fabricated from PEO of 10wt% spun at 10000 RPM has diameter in the range of 1µm to 5µm.This demonstrated that the spinning rate determines the size of fiber diameter despite that the concentration of PEO of 10wt% was higher than the PEO 8wt% . PVP 24wt% in solution yielded fiber at 7000 RPM with fiber diameter in the range of 5µm to 35µm. The large diameter is due to the high concentration of PVP solution and also the RMP that yielded good fiber which was 7000RPM. Low fiber diameter would have been produced if the PVP solution of 24%(w/w) would have yielded fiber at higher RPM. This is to buttress the point that fabricated parameters are very important during nanofiber production. The chosen parameters determine the morphology of the nanofiber.

The nanofibers diameter distribution as shown in Figure 22 (a) where the PEO 8% (w/w) has a mean diameter of 5.24 mm and standard deviation of 2.26. The PEO 10% (w/w) in figure 3 (b) shown nanofiber diameter mean value of 2.85mm and standard deviation value of 0.85. The lower diameter of this nanofiber is due to the higher rotational speed of the spinneret which among the intrinsic properties that controls the fabricated nanofiber diameter.

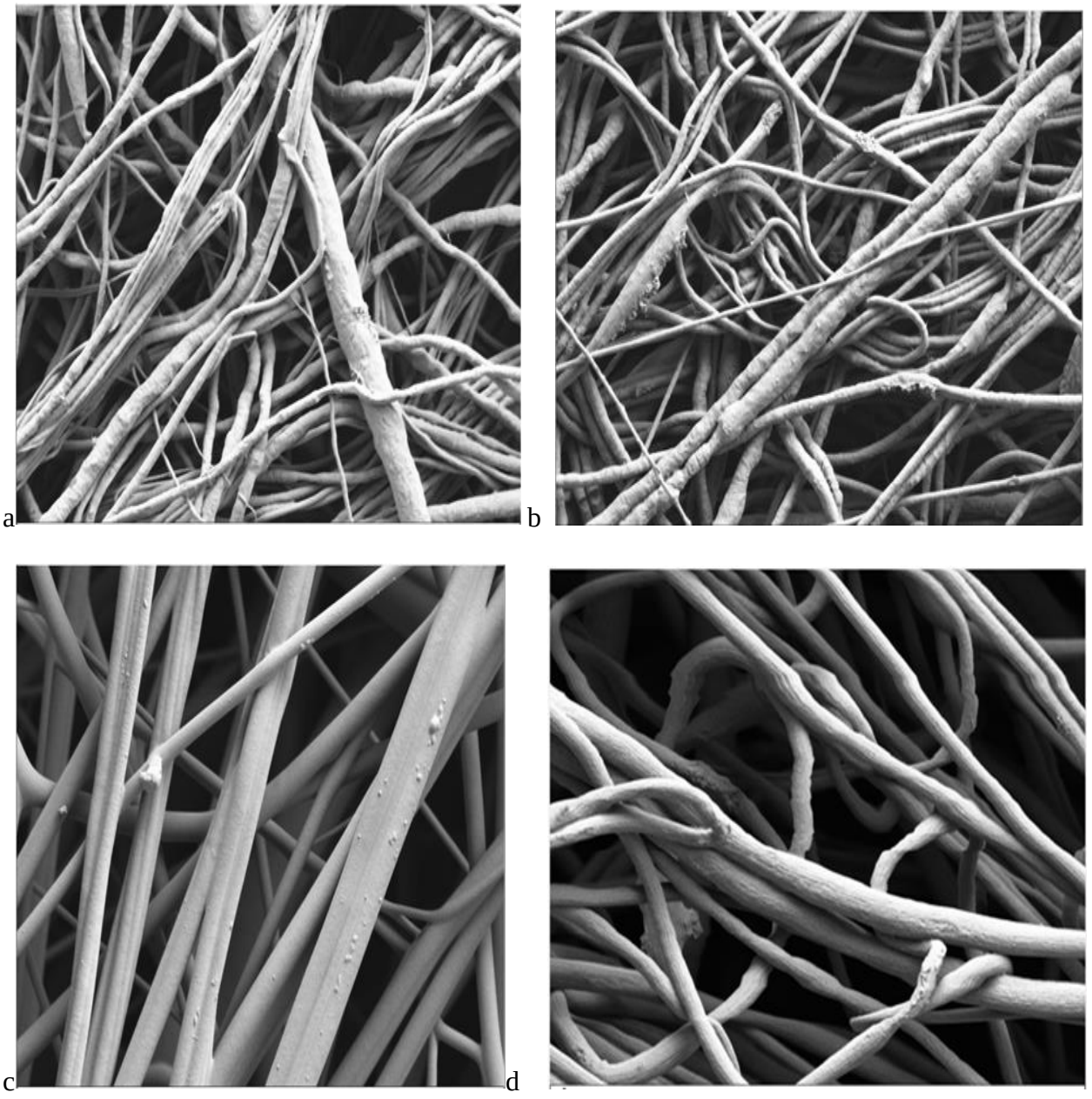

Figure 21 (a) SEM image of PEO 8% (w/w) at 5.0K magnification (b) SEM image of PEO 10% (w/w) at 5.0K magnification(c) SEM of PVP 24%(w/w) at 5.0K magnification (d) SEM image of PEO: PVP 12%: 12% (w/w)

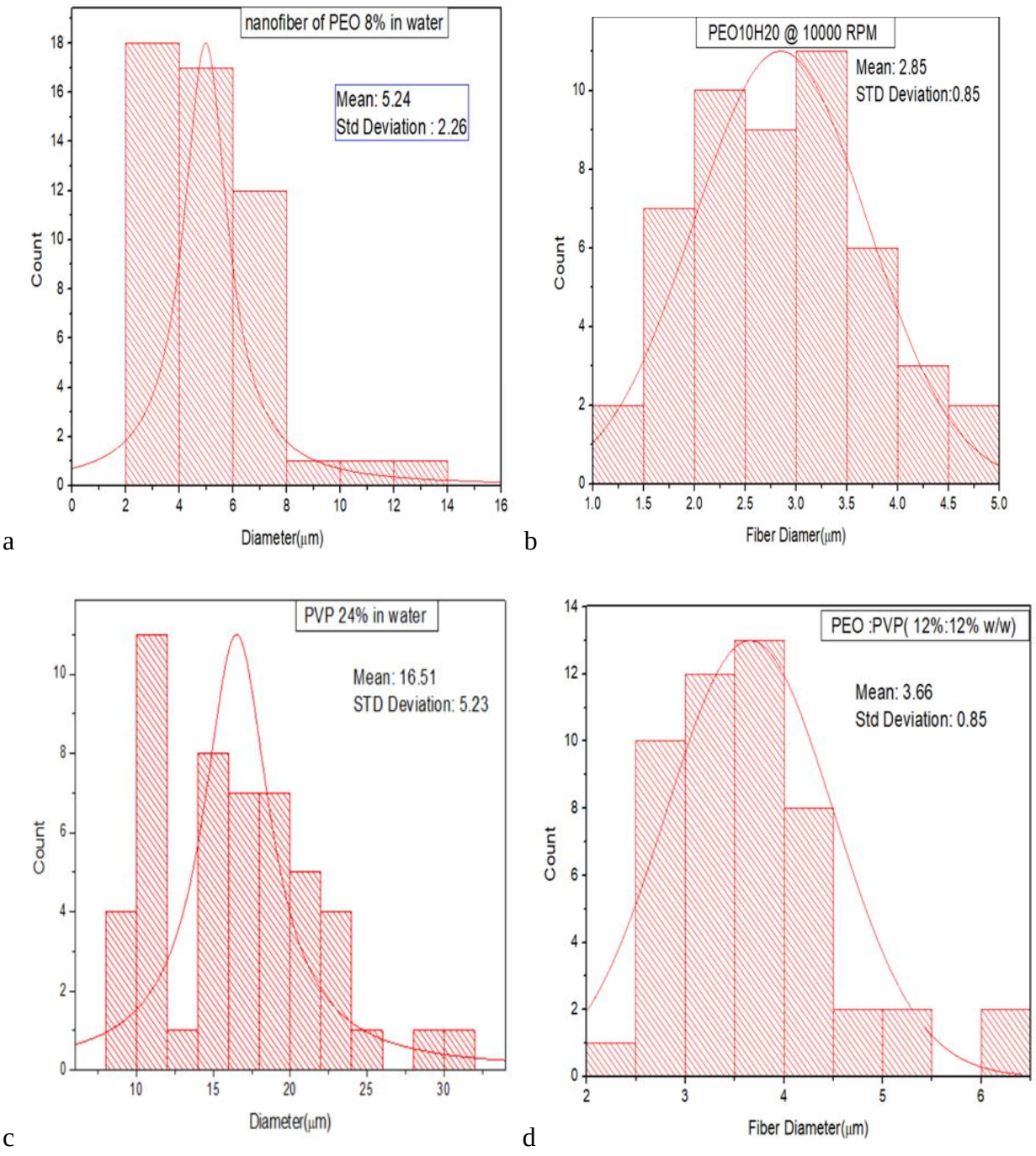

Figure 22 Nanofiber diameter distribution curve (a) PEO 8% w/w (b)PEO 10% w/w (c) PVP 24% (w/w) (d) Co-nanofiber PVP:PEO (12% :12%)

FTIR spectra(a) PEO bulk samplePEO nanofibers, PVP nanofibers, PEO -PVP co nanofibers

The FTIR spectra as shown in Figure 23. gave absorption bands of PEO bulk sample. PEO nanofibers, PEO and PVP co-polymers nanofibers. There is a strong band around 2900cm^{-1} which is due to the asymmetric and symmetric C-H stretching modes in PEO. The bands between 1470 cm^{-1} and 1330 cm^{-1} are due the vibrations of -CH2- group in the PEO. The bands at the range of 1350 cm^{-1} to 1090 cm^{-1} are primary O-H in-plane bend. The bands at about 1154 cm-1 to 940 cm-1 are due to asymmetric stretching vibration of the C-O group. The bands from 950 cm^{-1} to 830 cm^{-1} are due to the Vinyl C-H out of plane bend. a shift at 1700cm^{-1} on the spectra of the nanofibers from PEO based polymer this is due to C-O the interaction of the hydrophilic end of the polymer with water.

The broad absorption band from 3600cm^{-1} through 3200cm^{-1} is due to the amine group in the polyvinylpyrrolidone. The absorption bands of 2900 cm^{-1}-2800 cm^{-1} is attributed to both the symmetric and asymmetric stretching of CH2. The bands in the absorption regions of 1400 cm^{-1} to 1300 cm^{-1} corresponds to CH deformation modes from the CH2 group. The bands with absorption of 1290 cm^{-1} to 1300 cm^{-1} is attributed to C-N bending vibration from PVP. The spectra of the PVP indicated that the molecular structure of the polymer is still retained after spinning for fabrication of nanofibers.

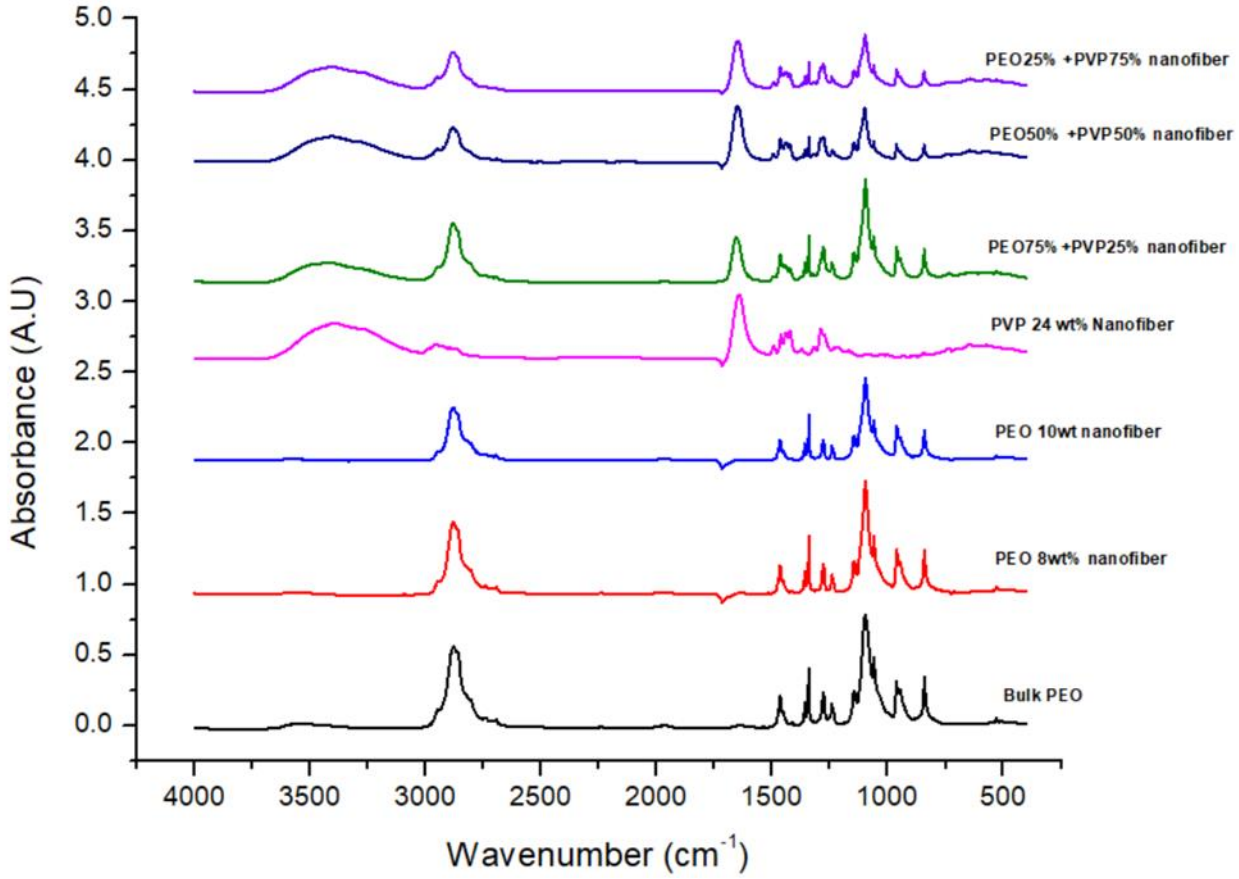

Figure 23. FTIR spectra of PEO bulk sample, PEO nanofibers, PVP nanofibers, PEO -PVP co nanofibers

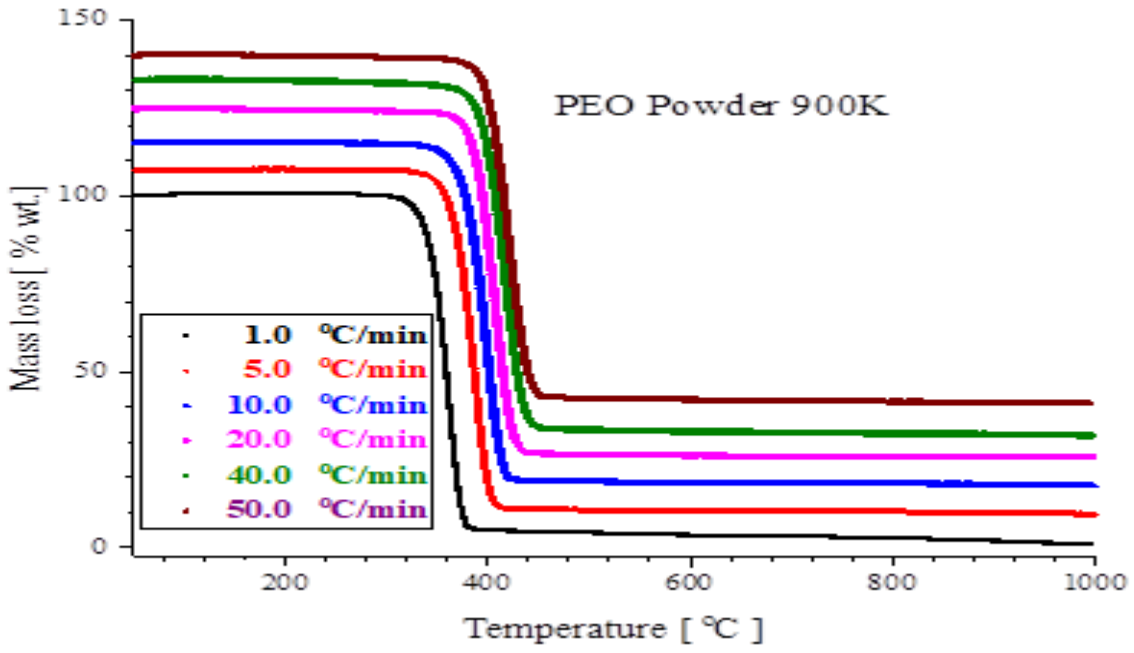

Figure 24. A plot of mass loss as function of Temperature on PEO powder, with a molecular mass of 900 K, recorded at various heating rates ranging from 1.0 to 50.^{0}C/min.

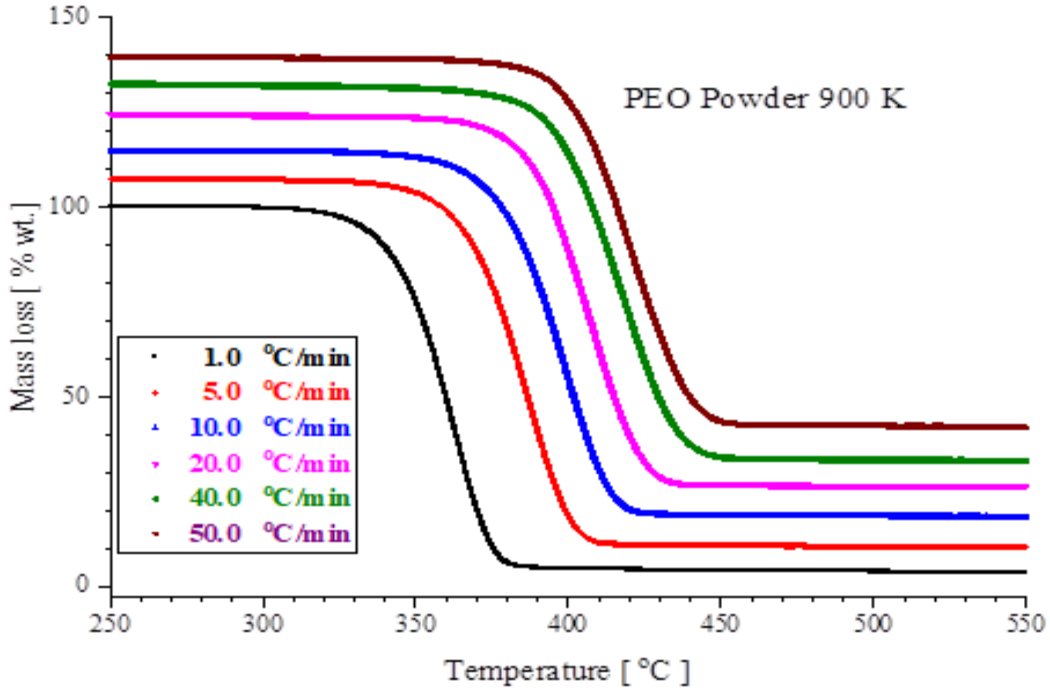

Figure 25. Represents a magnified figure of Fig.24, for the temperature range 250^{0}C to 550^{0}C. It is noticed that as the heating rate is increased the thermograms are shifted to higher temperatures.

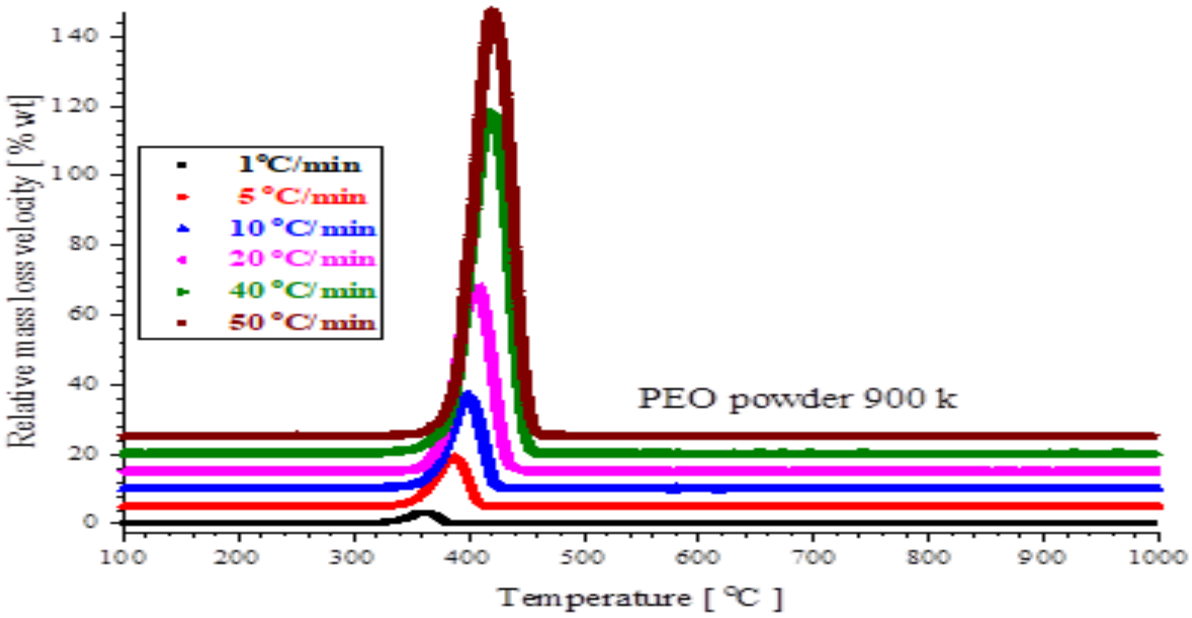

Figure 26. Derivative of the thermograms versus the temperature, of PEO powder for various heating rates

It is noticed that all thermograms of the PEO powder are showing a single maxim, suggesting a single main degradation process .The position of the maxim defines the temperature at which the mass loss is maximum or the position of the inflection point in the representation mass loss versus temperature

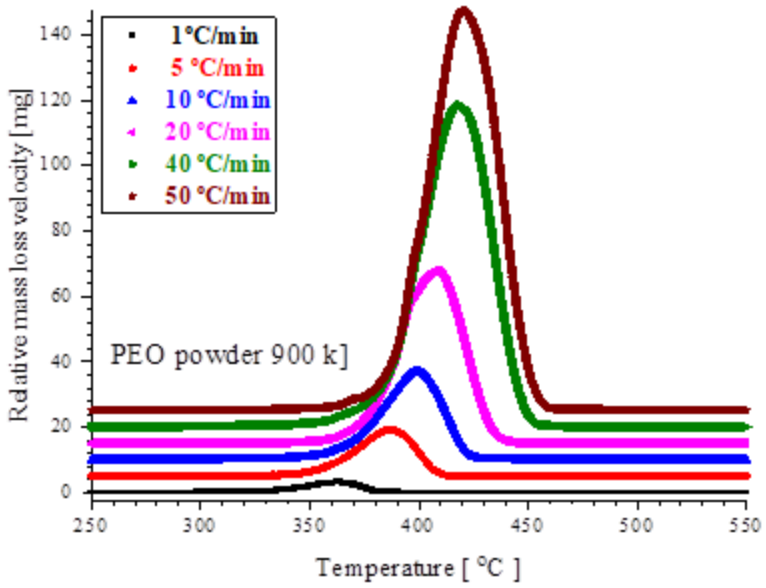

Figure 27. Represents a magnification of dependence shown in Figure.26 over the temperature range 250 to 550^{0}C.

Now it is easier to notice the effects of the heating rate. The increase of the heating rate shifts the position of the temperature at which the thermal degradation speed is highest to higher temperature, narrows the distribution of the relative mass loss velocity versus the temperature and increase the amplitude of the relative mass loss peak. Eventually it is noticed that the thermograms are slighty asymmetric; it is speculated that actually there is a very small difference between the degradation of PEO in the amorphous and in the crystalline domains, which broadens the dependencies shown in Figures 26 and 27.

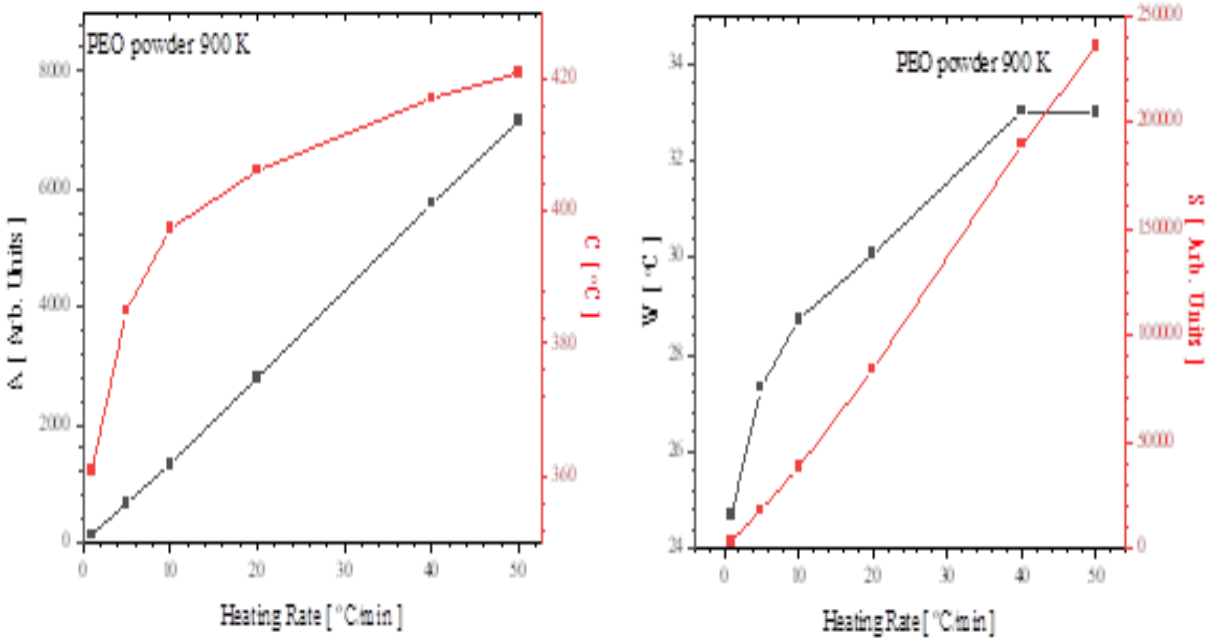

Figure 28. The dependence of A and C on the heating rate .B. right. The dependence of W and S on the heating

A more detailed mathematical analysis was performed on the derivative of these thermograms. From Figures 26 and 27 it may be concluded that the derivative of the thermograms depend on temperature as a Lorentz distribution. Although a weak asymmetry may be noticed, all these derivatives exhibit a single maximum, suggesting that these dependences may be simulated by

using a single Lorentzian line. This was performed using Origin Pro simulation capabilities in C-Program, corresponding to the expression:

y=B+S*x+(2*A/PI)*(W/(4*(x-C)*(x-C)+W*W))

Where y is actually the residual mass at a given temperature C, B is the zero base line, S describes the slope of the thermogram's derivative, A is the amplitude of the derivative, W is the width of the Lorentzian and C is the position of the maximum mass loss velocity (on the OX or temperature axis). The fits were very good and provided the most important parameters, A, W, and C. The integral of the Lorentzian line, S, was also estimated, assuming that the heating rate does not affect the shape. The quantities are collected in the graphs 28A and 28B, respectivel

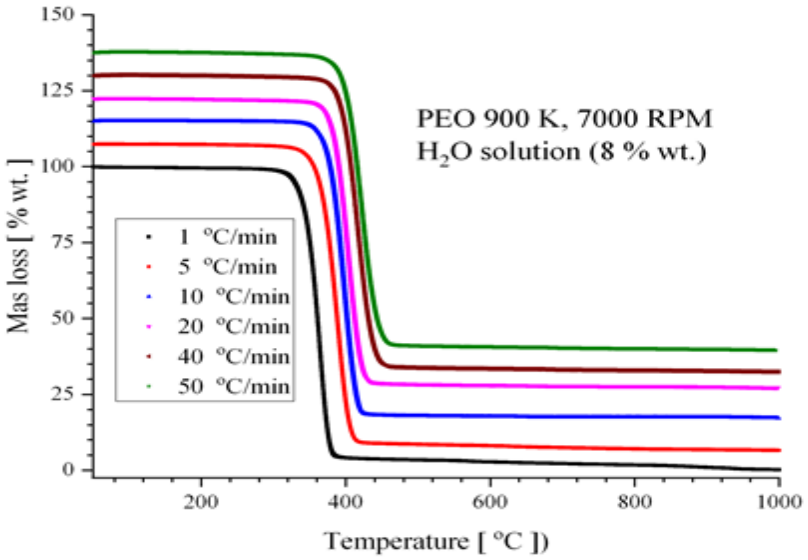

Figure 29. A plot of mass loss as a function of Temperature of PEO-based nanofibers fabricated from PEO in water 8% (w/w) at 7000 rotational per minute.

It is noticed that the increase of the heating rate on PEO based nanaofibers shifts the position of the temperature at which the thermal degradation speed is highest to higher temperature.

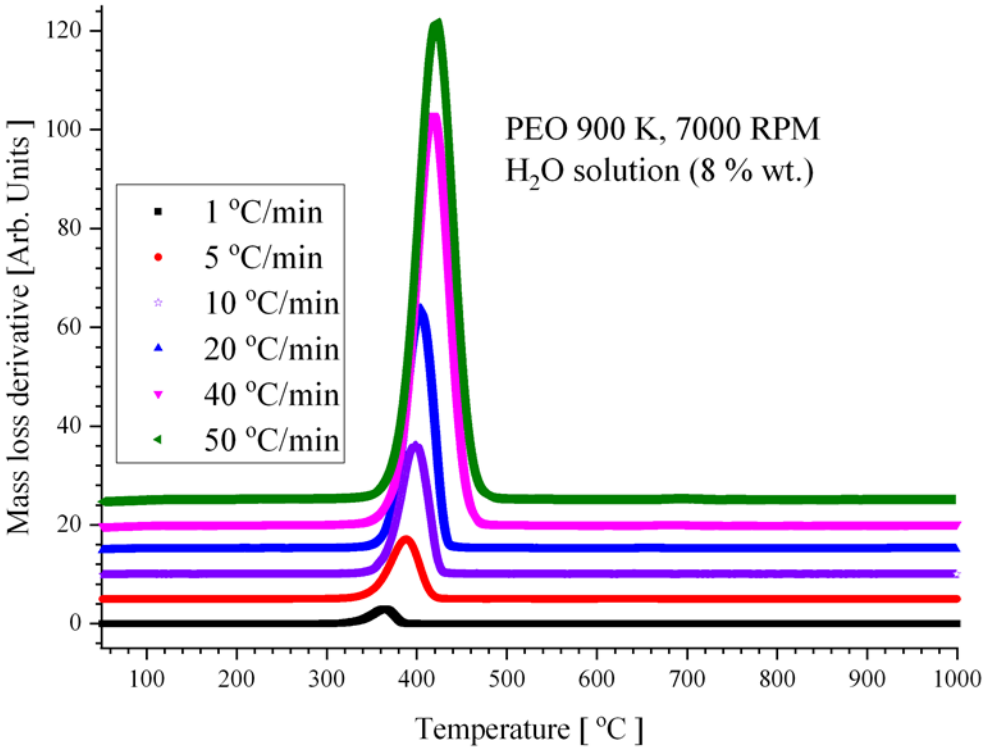

Figure 30. Derivative of the thermograms versus the temperature, of PEO-based nanofibers fabricated from PEO solution 8%, w/w for various heating rates

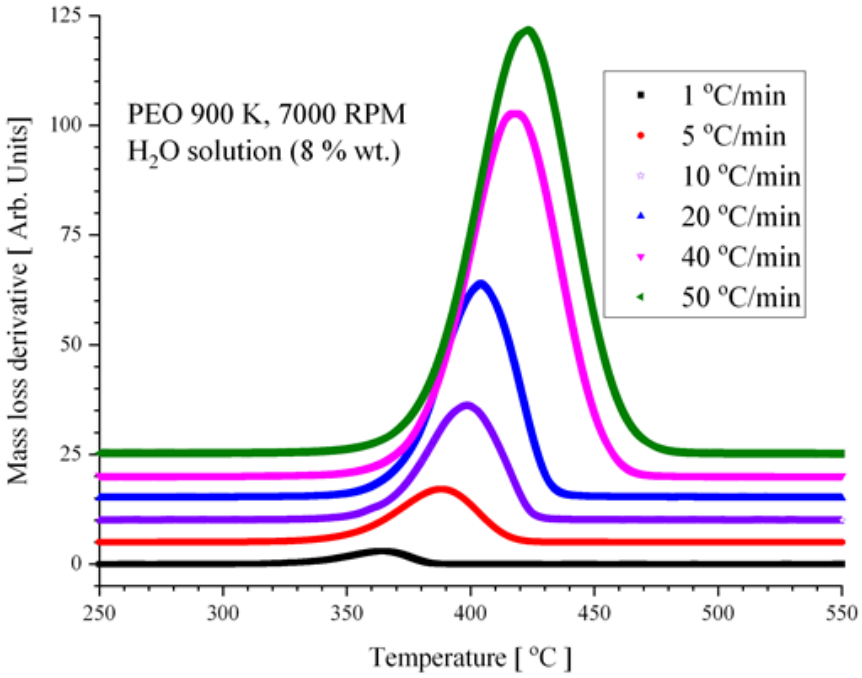

Figure 31. Magnified copy of figure 30. Showing derivative of the thermograms versus the temperature, of PEO-based nanofibers fabricated from PEO solution 8%, w/w for various heating rates.

The thermogram from the PEO nanofibers in figure 30, shows the effects of the heating rate on the nanofibers. The increase of the heating rate shifts the position of the temperature at which the thermal degradation speed on is highest PEO nanofibers to higher temperature, narrows the distribution of the relative mass loss velocity versus the temperature and increase the amplitude of the relative mass loss peak. Eventually it is noticed that the thermograms are is also slightly asymmetric as it occurred in the PEO powder. Figure 31 is included for clearer image of the thermogram.

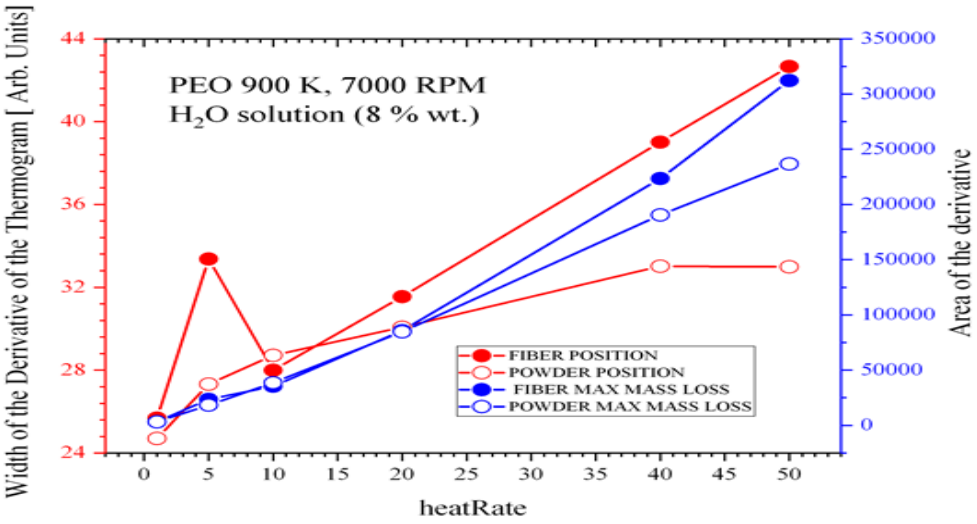

Figure 32A. Width of the derivative as function of the heating rate

It is noticed that as the heating rate is increased the width of the derivative of the thermogram is also increased for the nanofibers and the PEO powder.

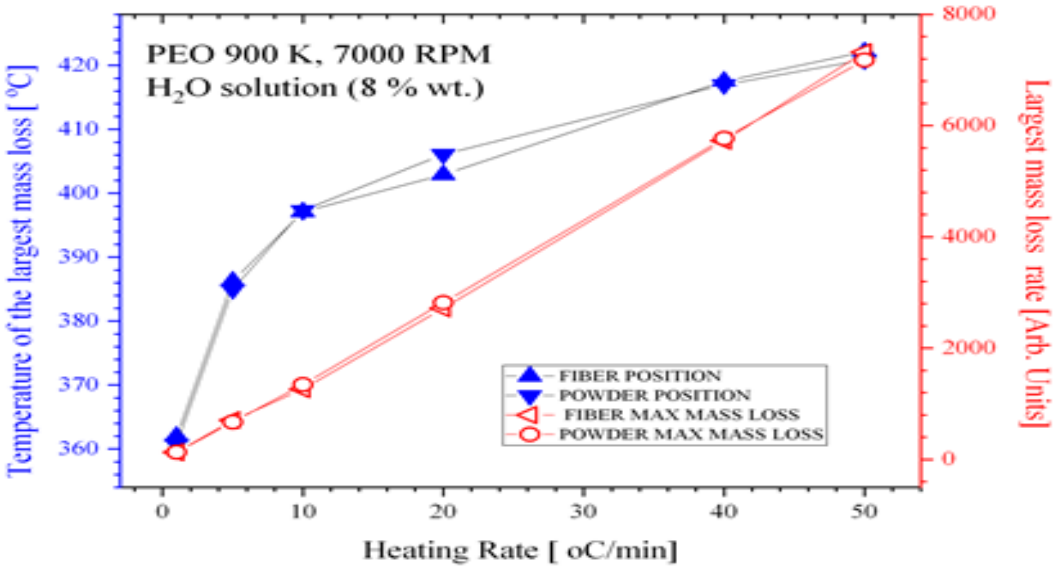

F**igure 32B** Temperature of the largest mass loss as function of heating rate.

It is noted that the temperature of the largest mass loss occurred at the highest heating rate and also the largest mass loss rate occurred at the highest heating rate.

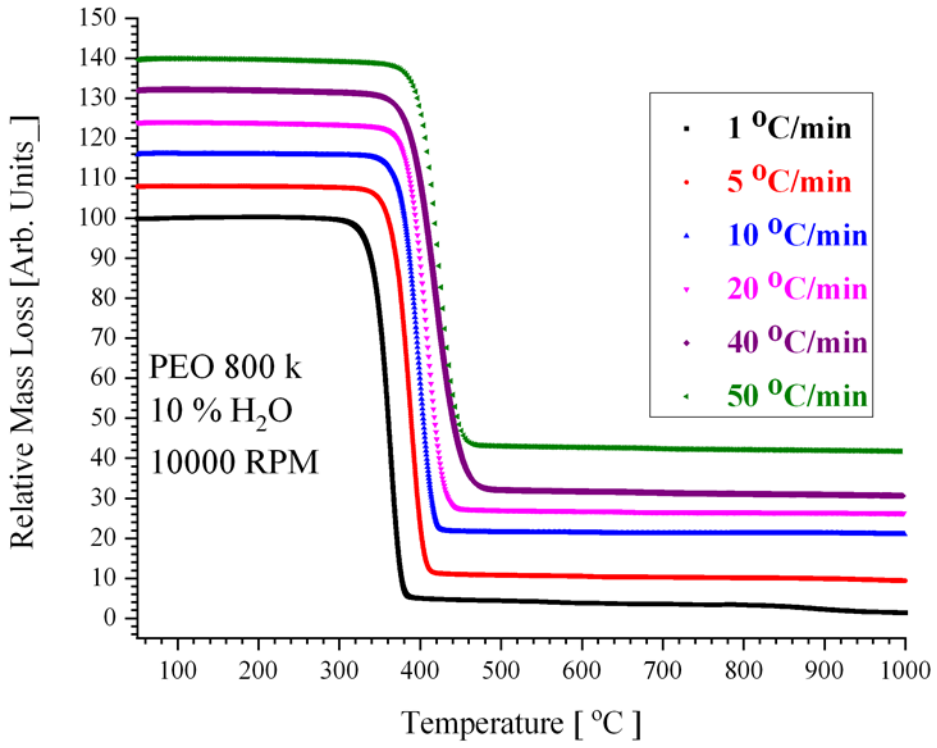

Figure 33. A plot of mass loss as a function of Temperature of PEO-based nanofibers fabricated from PEO in water 10% (w/w) at 10,000 rotational per minute.

The thermogram from the PEO nanofibers fabricated from 10% (w/w) solution at 10,000 rotational speed per minute (RPM) in figure 33, also shows the effects of the heating rate on the nanofibers. The increase of the heating rate shifts the position of the temperature at which the thermal degradation speed on is highest PEO nanofibers to higher temperature, narrows the distribution of the relative mass loss velocity versus the temperature and increase the amplitude of the relative mass loss peak. Eventually it is noticed that the thermograms are is also slightly asymmetric as it occurred in the PEO powder.

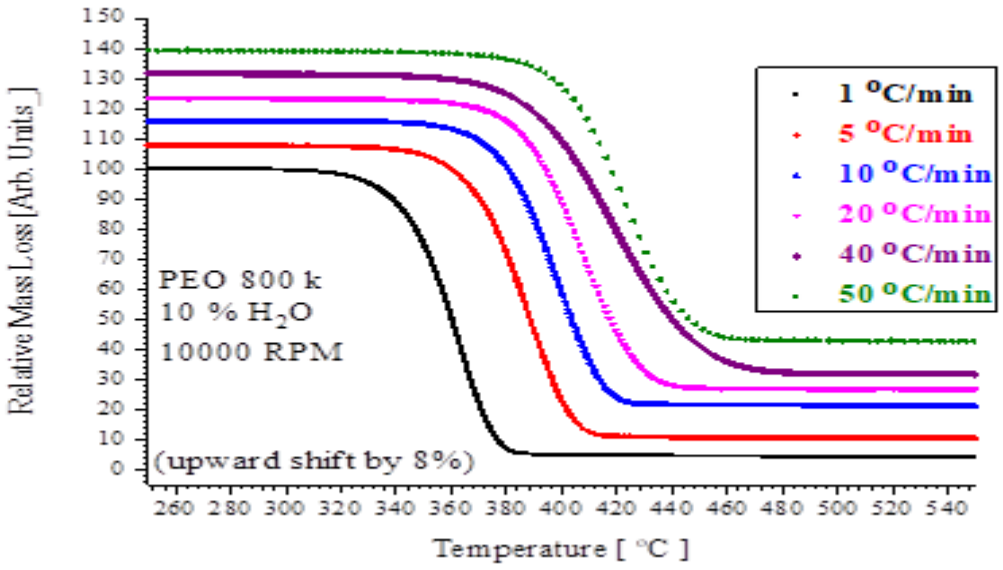

Figure 34. A magnified copy of figure 33 showing a clearer mass loss as a function of temperature.

From figure 34 is clearer that as the heating rate is increased , the degradation temperature of the nanofibers shifts to higher temperature.

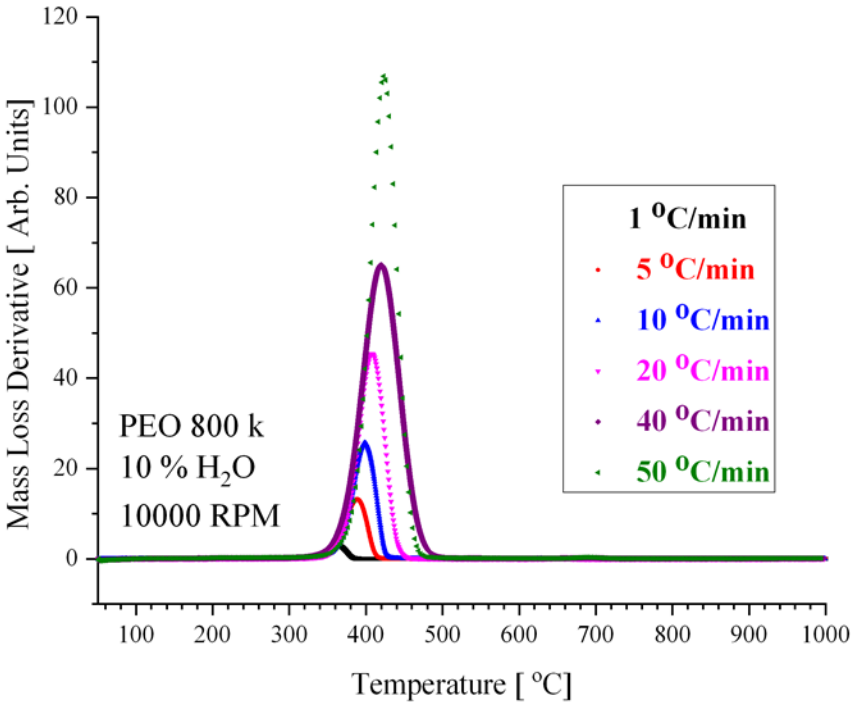

Figure 35. Derivative of the thermograms versus the temperature, of PEO-based nanofibers fabricated from PEO solution 10%, w/w at 10,000 RPM at various heating rates.

The largest mass loss occurred at the highest heating as indicated in figure 35.

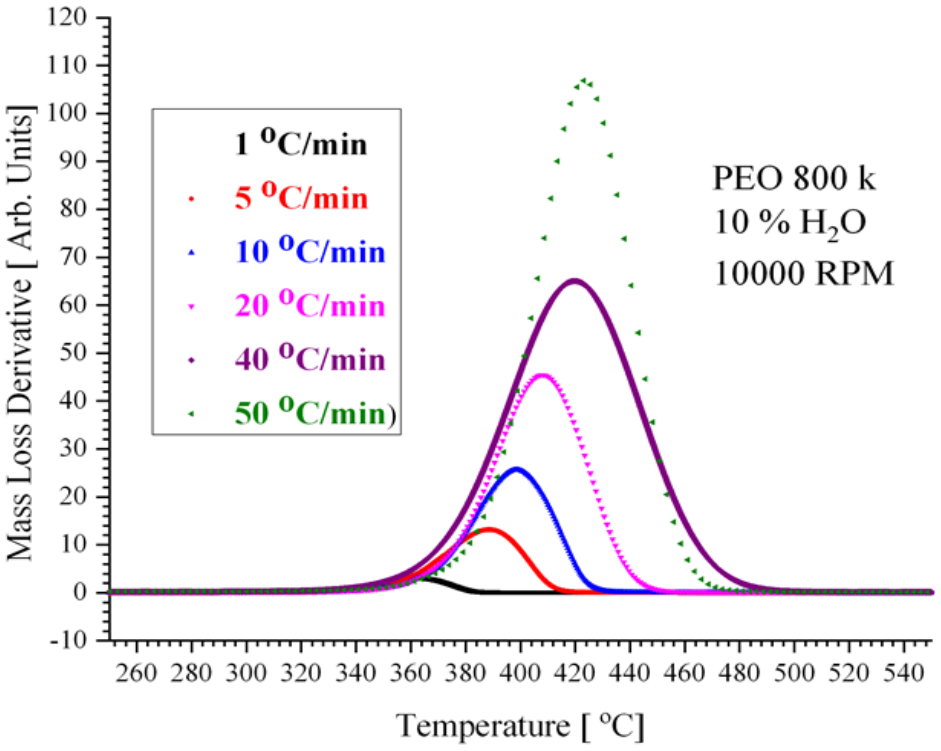

Figure 36. Magnification of figure 35 thermograms versus the temperature, of PEO-based nanofibers fabricated from PEO solution 10%, w/w at 10,000 RPM at various heating rates for clarity purpose..

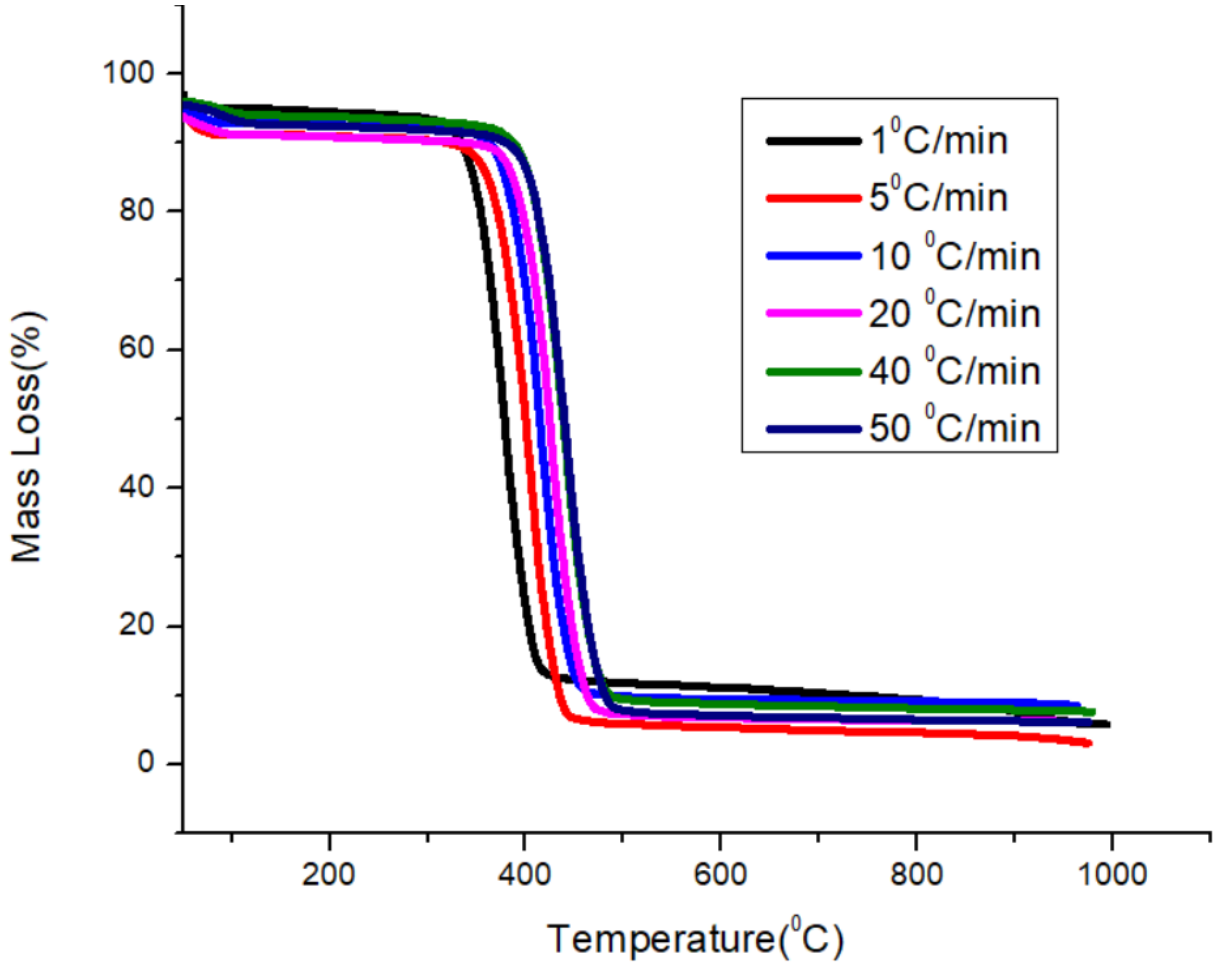

Figure 37 TGA thermogram of co-nanofibers PEO 12% + PVP 12%

The PEO and PVP co-nanofibers thermograms as shown in figures 37 and 38 indicate the increase of the heating rate shifts the position of the temperature at which the thermal degradation speed on is highest PEO and PVP co-nanofibers to higher temperature.

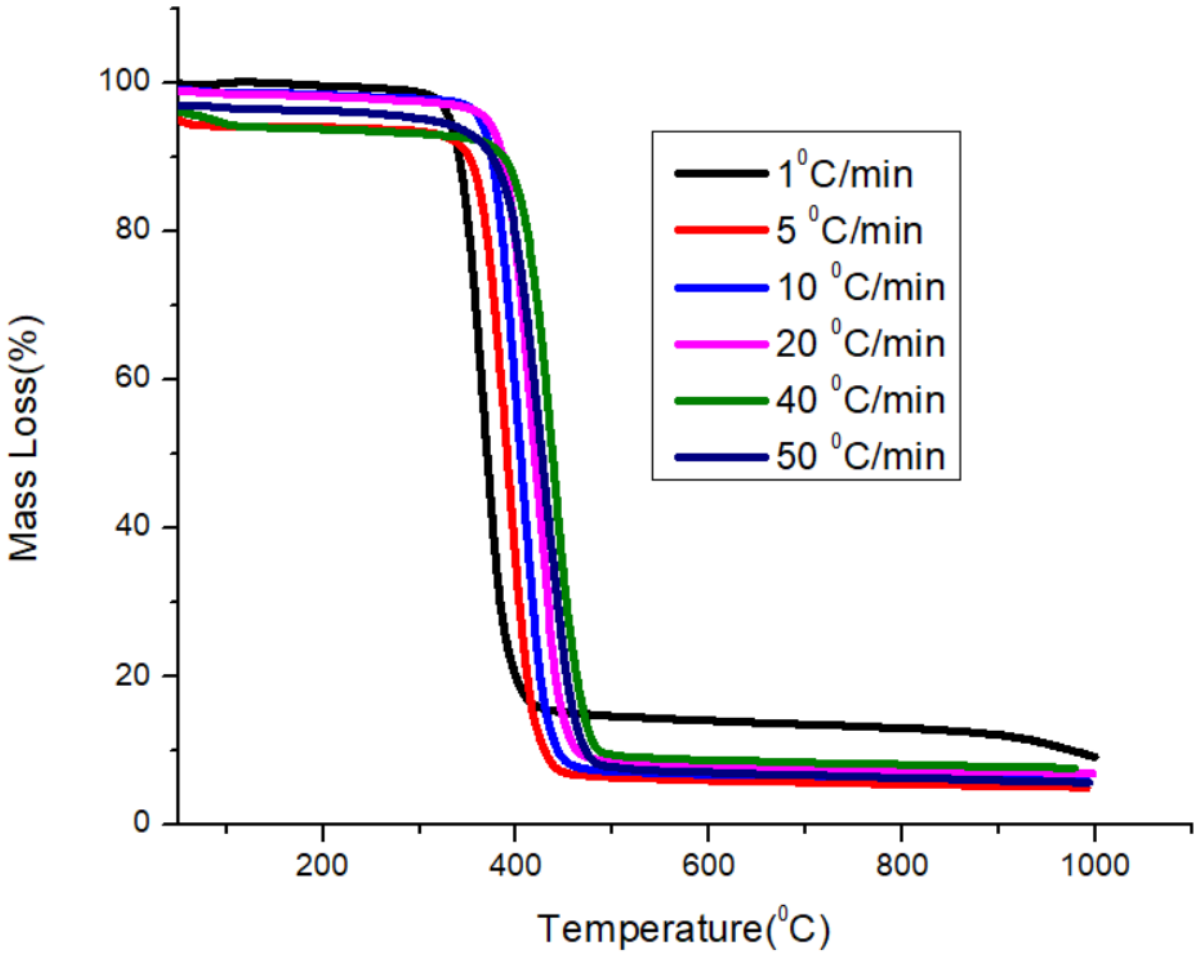

Figure 38 TGA thermogram Co-nanofibers of PEO75% + PVP 25 %

The cooling branch of Differential Scanning Calorimetry (DSC) reflects crystallization processes. As may be noticed from figure 39,the melting of the PEO powder at various heating rates is represented by a single slightly asymmetric function, that may be approximated by a Lorentzian, for all heating rates investigated (ranging from 1 to 60^{O}C/min). The weak asymmetry

is better seen at a heating rate of 10^{O}C/min. The DSc plots of the crystallization processes are affected by the cooling rate.

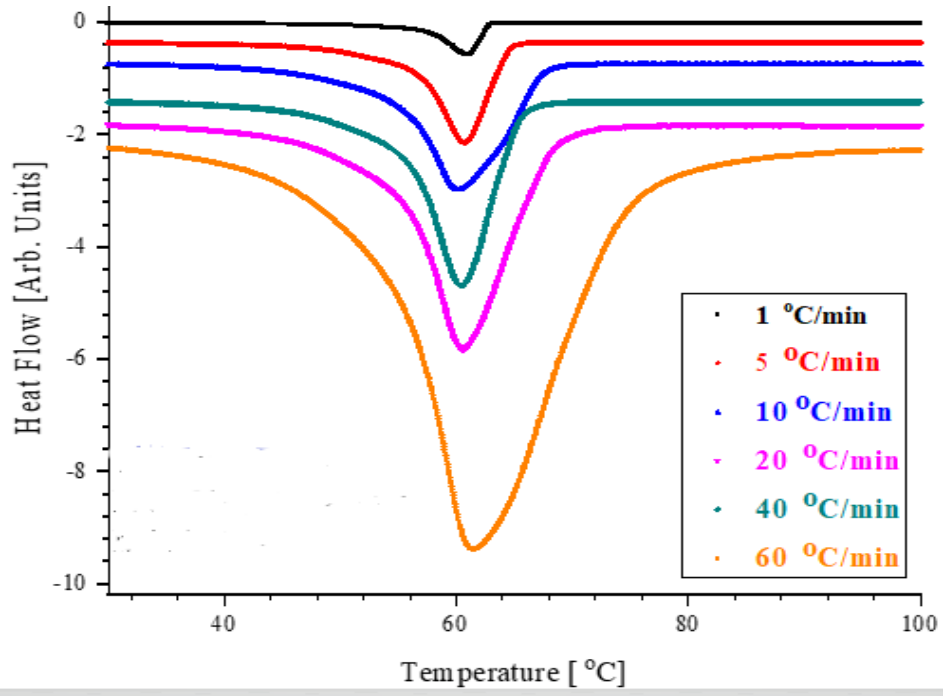

Figure 39. DSC of PEO powder (melting branch) showing the melting of crystallites for pristine PEO powder at various heating rates.

It is observed that the maximum heat flow to the polymer increases as the heating rates is increased. The width of these dependencies are almost constant as the heating rate is changed. The crystallization temperature T_{Cryst} represented by the temperature at which the heat flow is maxim, exhibits a complex dependence on heating rate, with a minimum of about 60^{O}C at a heating rate of 10^{O}C/min. This may suggest two competing crystallization mechanisms with close energies of activation.

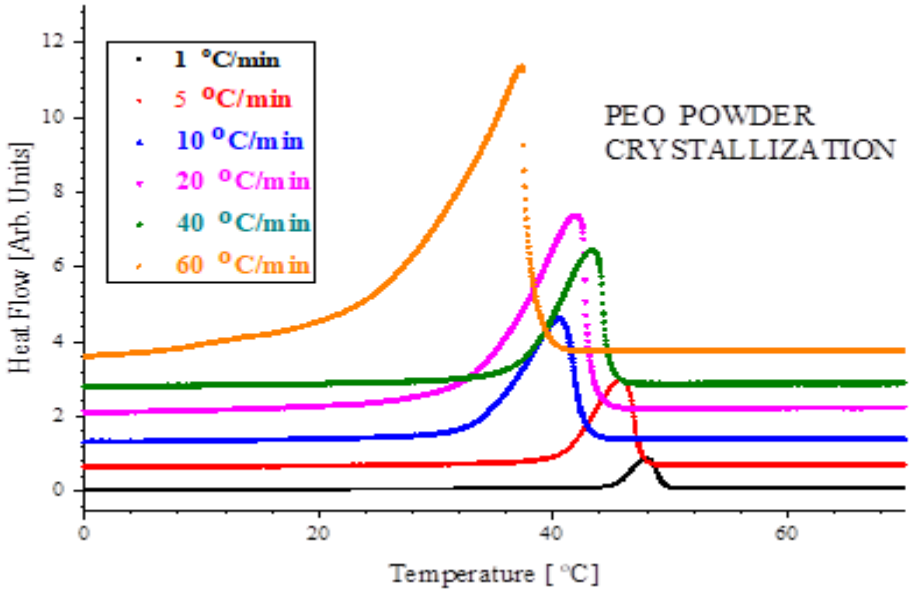

Figure 40. The crystallization of PEO powder at various heating rates

Figure 40 emphasizes on the crystallization process in PEO powder at various heating rates. Excepting the opposite sign of the process, because the heat flow is reversed in the recorded thermograms are single asymmetric Lorentzian lines. While the changes in the width of the crystallization process are within the experimental errors, the amplitude of the heat transfer is increased as the cooling rate is increased. As noticed from figure 40 and figure 41, the lowest crystallization temperature is about $37^{O}C$ and the highest one about $48^{O}C$. Qualitatively both crystallization and melting show similar dependencies on the heating rate, with a break at about $10^{O}C$/min.

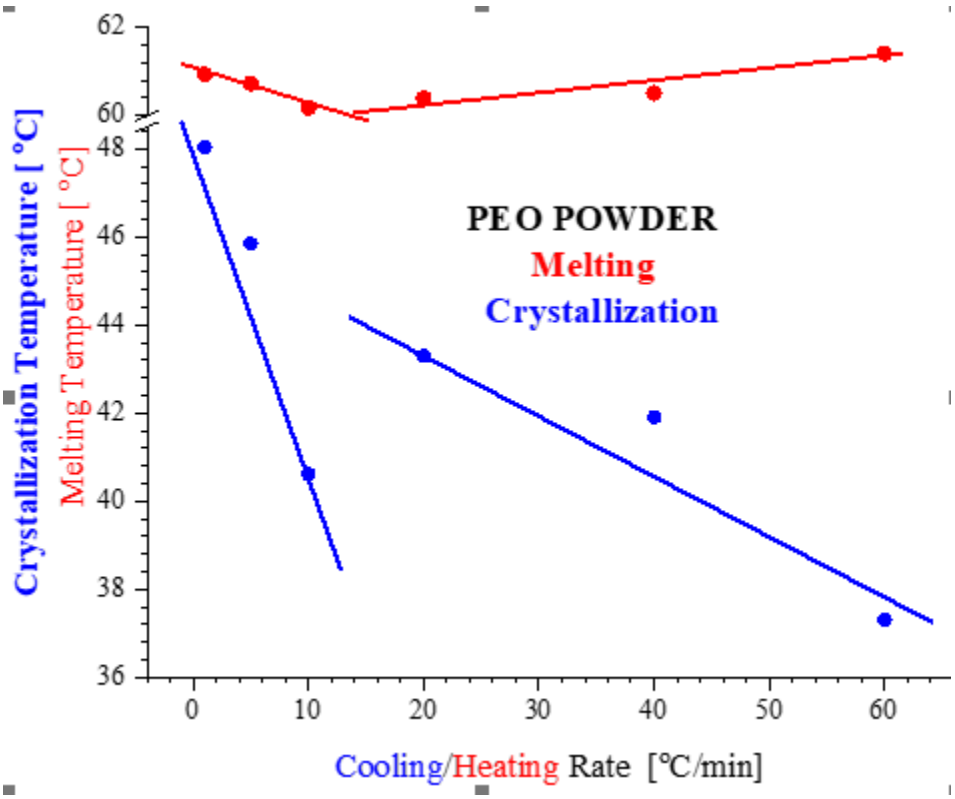

Figure 41. The dependence of the melting and crystallization temperatures on the heating rate for PEO powder

Figure 42 shows the Glass Transition temperature (T_g) at different heating rates. At a heating rate of 1^{O}C/min, the transition is too weak and cannot be observed. As the heating rate is increased, the Glass Transition temperature shifts to higher temperatures and is enhanced. At a heating rate of 40^{O}C/min the Glass Transition temperature of PEO powder is -61.5^{O}C, in agreement with literature. Cooling shifts the glass transition towards lower temperatures, moving the transition beyond the range of temperatures accessible for the DSC spectra.

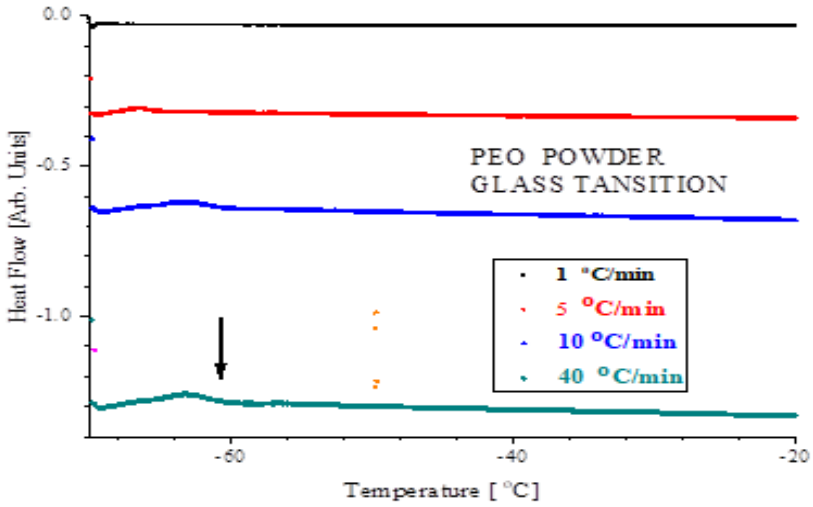

Figure 42 . Glass transition temperature in PEO powder, for different heating rates

Figure 43. shows that the crystallization process in PEO nanofibers obtained from Chloroform precursor solution is different from the crystallization process of the PEO powder. At a cooling rate of 1^{O}C/min, the heat flow as a function of temperature shows a single asymmetric Lorentzian.

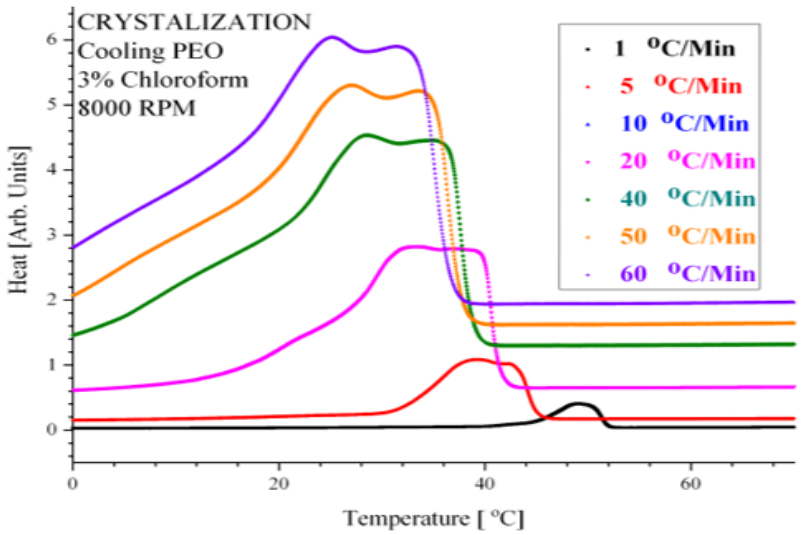

Figure 43. Crystallization process in PEO nanofibers obtained from Chloroform solution precursor.

As the heating rate is increased, it becomes clear that the crystallization process is a superposition of two processes as shown in figures 43 and 44.

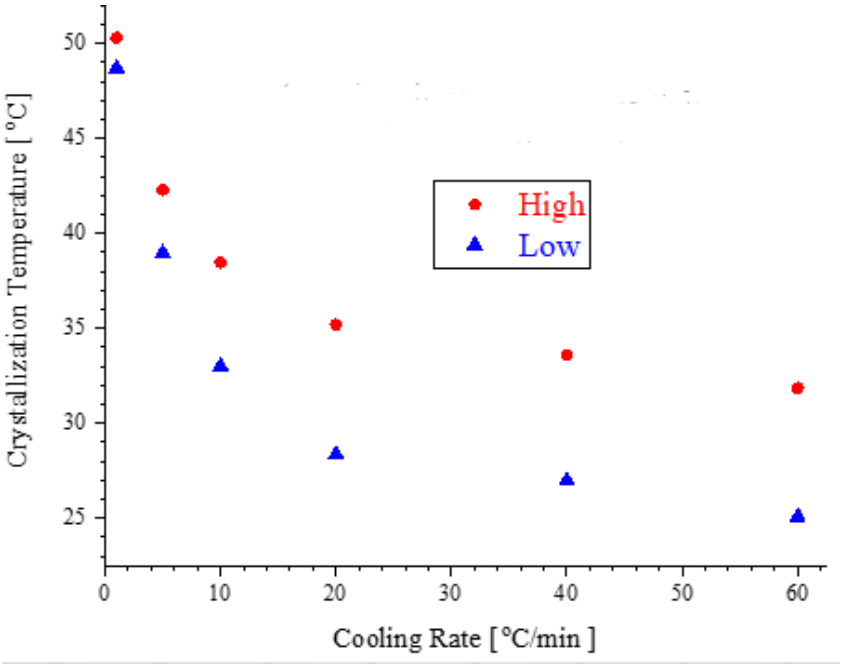

Figure 44. Dependence of the high (red) and low (blue) crystallization temperature on cooling rate of PEO nanofibers from 3 % w/w in Chloroform at 8000RPM.

The increase of the cooling rate enhances the heat flow and shifts the crystallization temperatures to lower temperatures.

Figure 44. represents the dependence of the two crystallization temperatures (defined by the peaks of the heat flow) on the cooling rate.It is noticed that as the heating rate is decreased the difference between the two crystallization temperature is decreased, an asymptotic crystallization

temperature of about 53^{O}C is suggested for PEO nanofibers obtained from Chloroform solution precursor. This is consistent with the crystallization temperature of bulk PEO. However, in this case,the dependence of the crystallization temperature (both high and low) is monotonous for all the heating rates. The crystallization temperature is decreased as the heating rate is increased. The reason for the two crystallization processes is that as the chloroform evaporates very fast, the crystallization starts while the polymer solution is flying towards the collector. This crystallization occurs on the surface of the nanofibers; However, the crystallization is not completed when the polymer reached the collected, hence a second crystallization, of the core of the nanofibers is taking place, completing the final crystallization of the nanofiber.

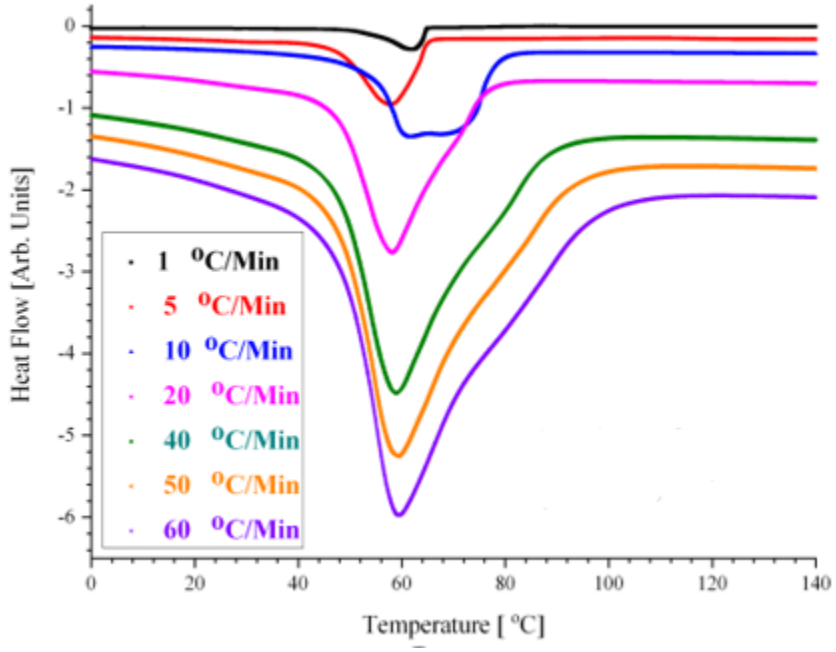

Figure 45. The dependence of the melting temperature for PEO nanofiber obtained from Chloroform precursor solution on temperatures for various heating rates

As noticed in figure 45, the dependence of the heat flow on temperature for the heating branch (melting) does not show two components, but rather an asymmetric heat flow that may suggest two crystallization processes with close activation energies. The position of the melting temperature is almost independent on the heating rate (for heating rates larger than 10^{O}C/min), the estimated melting temperature is about 60^{O}C.

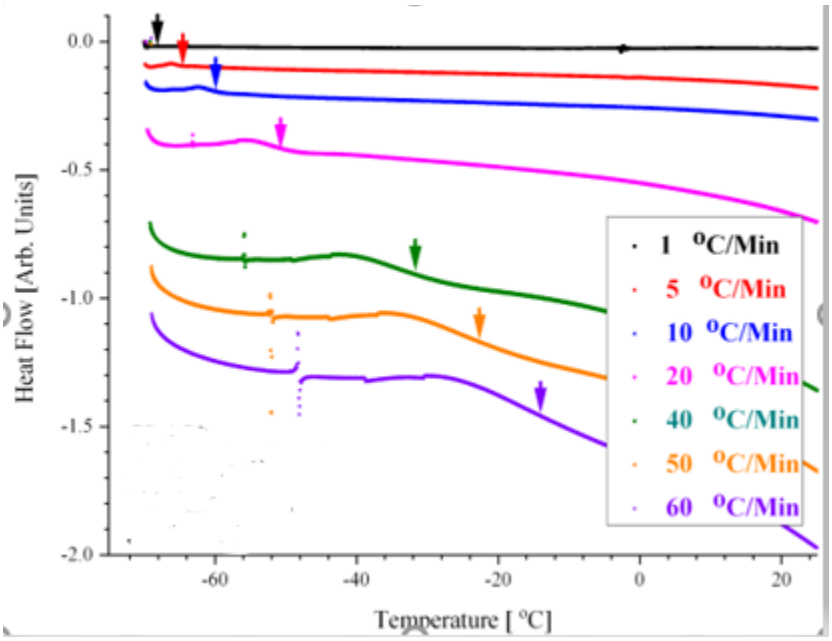

Figure 46. The dependence of glass transition temperature on the heating rates for PEO nanofibers obtained from Chloroform solution precursor at 8000RPM

Figure 46 represents the heat flow for various heating rates, within the glass transition temperature. A strong dependence of the glass transition temperature on the heating rate is observed. As noticed from figure 47, the dependence of the glass transition temperature on the heating rate is linear, allowing the estimation of an asymptotic transition temperature of -74^{O}C. This value is in good agreement with literature.

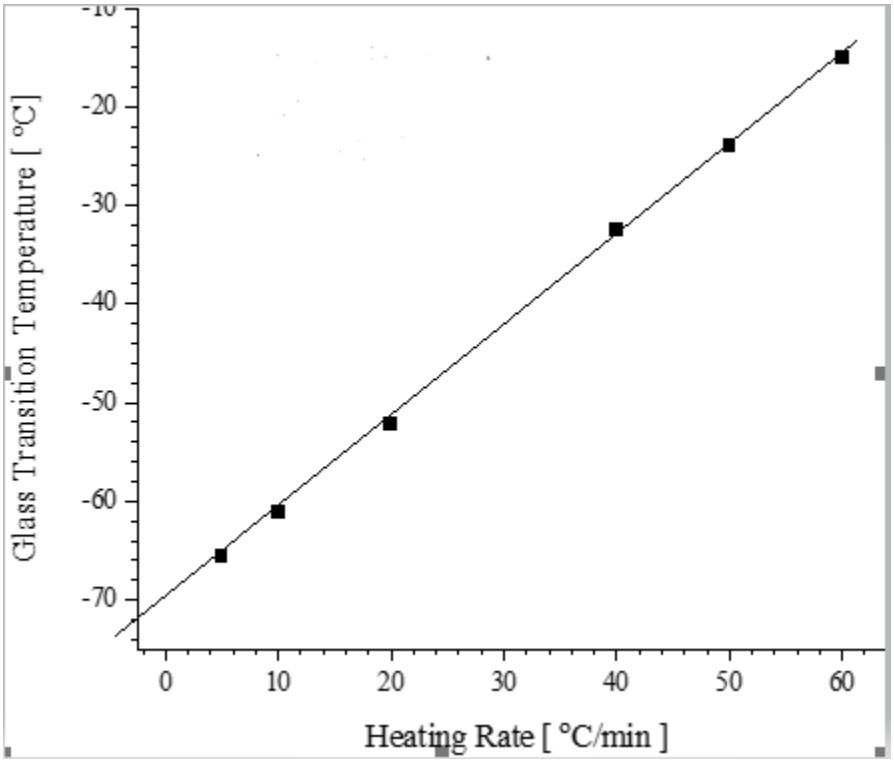

Figure 47. The dependence of glass transition temperature on the heating rate in PEO nanofibers obtained from Chloroform precursor.

Figure 48. shows the heat flow for the crystallization process occurring in PEO nanofibers obtained from water solutions precursors. As in previous cases, it is noticed that the heat flow is enhanced as the heating rate is increased. For PEO nanofibers obtained from water solutions, the heat flow associated to the crystallization process is quasi-symmetric. As the heating rate is increased, the crystallization temperature defined by the maxim of the heat flow, shifts to lower temperatures.

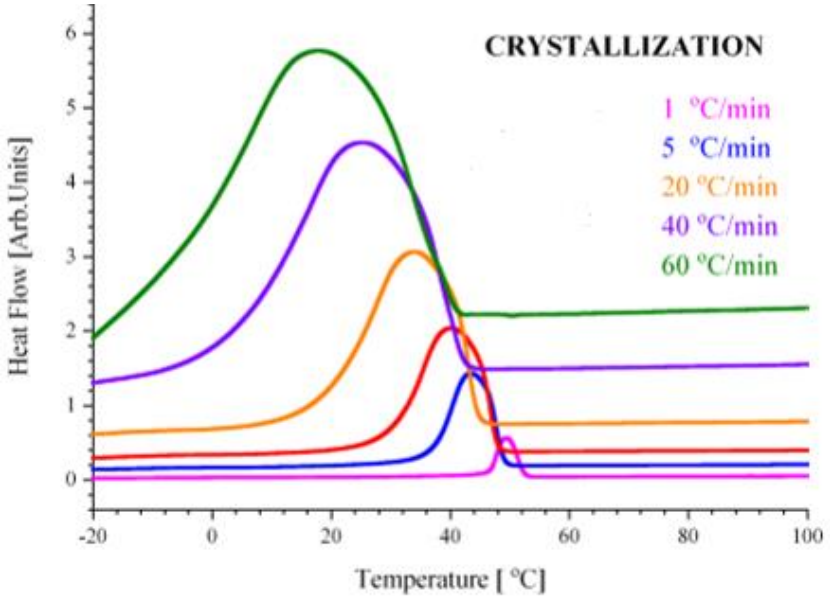

Figure 48. The heat flow for the crystallization process of PEO nanofiber obtained from water solution precursor (8% w/w) at 7000RPM

Figure 49 shows the heat flow for the melting of PEO nanofiber from water solution precursor at different heating rates. It is observed that as the heating rate is increased the melting temperature shift to higher temperature.

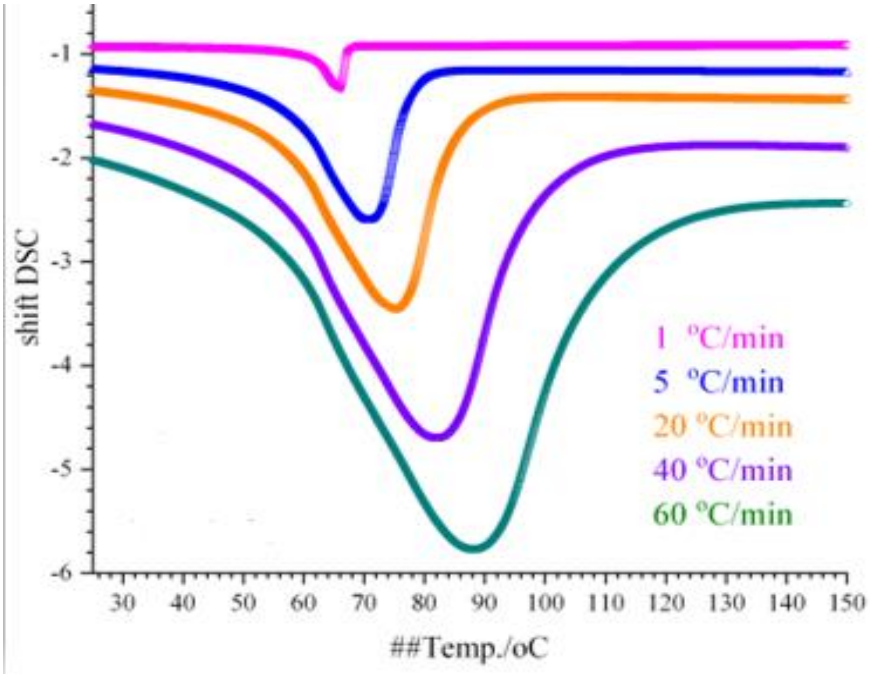

Figure 49. The heat flow for the melting of PEO nanofibers from water solution precursor.

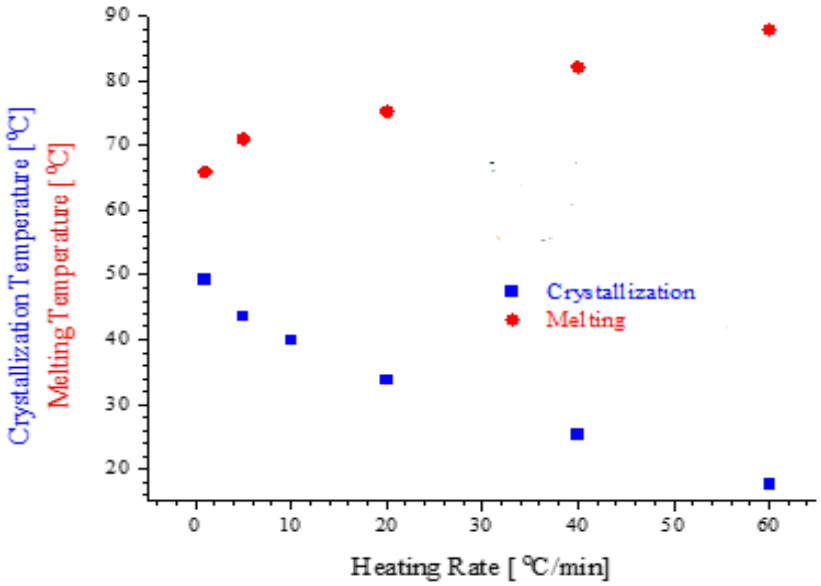

Figure 50. The dependence of crystallization and melting temperature on heating rates.

From figure 50, it is noticed that the crystallization temperature decreases as the heating rate increases and the melting temperature increases as the heating rates increases.

CHAPTER IV

SUMMARY AND CONCLUSION

The solutions of PEO (from 3% w/w to 10% w/w) PVP 24%(W/W) and co-solutions of PEO and PVP were prepared from PEO polymer of molecular weight 900,000 $g.mol^{-1}$ and PVP of molecular weight 1,300,000 $g.mol^{-1}$ respectively after optimizing the concentrations of the solution that could yield polymer-based nanofibers. The concentration of the polymer is a function of the molecular weight of the polymer and the amount of polymer used in making a specific solution. The surface tension was analyzed using Famas interface measurement analysis system. It is was demonstrated that the relationship between the surface tension and the polymer concentrations are inversely related.

The Forcespinning™ machine was used in fabricating the nanofibers by optimizing the operating conditions of the machine which involves using optima rotating speed of the spinnerent and also the distance of the standing collectors. The spun nanofibers were subjected to scanning electron microscopy to determine the morphology of the nanofiber which showed nanofibers of nice cylindrical morphology with smooth surface and a low concentration of beads. The diameter of the nanofibers was measured and distribution curve from histogram plotted revealed a single mode distribution with a maximum in the range of tenth to hundreds of microns, which was a function of the intrinsic parameters of the solutions and the operating parameter of the forcespinning machine. Thus, it is reported the dependence of the average diameter of the force spun nanofibers on the concentration of the PEO water solutions and on the spinning rate.

Similar studies were ignited on polyvinylpyrrolidone (PVP) nanofibers obtained by the force spinning of water solutions. Complementary microscopy data were obtained using the Scanning Electron Microscopy (SEM) Sigma VP Carl Zeiss, Germany). The as obtained micrographs supported the data obtained by optical microscopy. The studies are currently extended to nanofibers of blends of two polymers (PEO and polyvinylpyrrolidone). The elemental mapping capabilities of the SEM allowed a more detailed analysis of the blend, by mapping the distribution of nitrogen atoms (which are present solely in polyvinylpyrrolidone).

Thermogravimetric measurements were performed by using a TG 209 F3 Tarsus-Netzsch instrument operating under nitrogen atmosphere, in the temperature range 50^0C to 1000^0C. Measurements with different heating rates ranging from 1^0C /min up to 50^0C /min have been performed. The increase of the heating rate shifts the position of the temperature at which the thermal degradation speed is highest to higher temperature, narrows the distribution of the relative mass loss velocity versus the temperature and increase the amplitude of the relative mass loss peak. Eventually it is noticed that the thermograms are slighty asymmetric; it is speculated that actually there is a very small difference between the degradation of PEO in the amorphous and in the crystalline domains.

A more detailed mathematical analysis was performed on the derivative of these thermograms. It may be concluded that the derivative of the thermograms depend on temperature as a Lorentz distribution. Although a weak asymmetry may be noticed, all these derivatives exhibit a single maximum, suggesting that these dependences may be simulated by using a single Lorentzian line.

The DSC showed that the maximum heat flow to PEO polymer increased as the heating rate is increased. The crystallization temperature exhibited a complex dependence on the heating rate with minimum at about 60^{O}C/min which showed two competing crystallization mechanism with close energies of activation. The lowest crystallization temperature is about 37^{O}C and the highest is about 48^{O}C. It is inferred that the two competing crystallization depends on the heating rate but with a break at 10^{O}C/min. The transition temperature shifted to higher temperature as the heating rate is increased. It is showed that the lowest glass transition of PEO powder is -61.5 at heating rate of 40^{O}C/min which agreed with literature. The increase in cooling rate enhanced heat flow and shifted the crystallization temperature to lower temperature.

The FTIR suggested that the nanofiber of PEO indicated same spectra like the bulk polymer suggesting that the molecular structure of the nanofiber was not altered in the course of forcespinning. Thou there was a shift at 1700cm^{-1} on the spectra of the nanofibers from PEO based polymer this is due to C-O the interaction of the hydrophilic end of the polymer with water.

REFERENCES

[1] M. Thirugnanaselvam, N. Gobi, and S. A. Karthick, “SPI / PEO Blended Electrospun Matrix for Wound Healing , Fibres and polymers SPI / PEO Blended Electrospun Martrix for Wound Healing,” no. May, 2014.

[2] T. T. Yuan, P. M. Jenkins, A. Marie, D. Foushee, A. R. Jockheck-clark, and J. M. Stahl, “Electrospun Chitosan / Polyethylene Oxide Nanofibrous Scaffolds with Potential Antibacterial Wound Dressing Applications,” vol. 2016, 2016.

[3] U. C. Paul, D. Fragouli, I. S. Bayer, and A. Athanassiou, “Functionalized Cellulose Networks for Efficient Oil Removal from Oil – Water Emulsions,” 2016.

[4] Y. Huang, X. Zeng, W. Wang, X. Guo, C. Hao, and W. Pan, “Sensors and Actuators A : Physical High-resolution flexible temperature sensor based graphite-filled polyethylene oxide and polyvinylidene fluoride composites for body temperature monitoring,” *Sensors Actuators A. Phys.*, vol. 278, pp. 1–10, 2018.

[5] W. Li, Y. Pang, J. Liu, G. Liu, Y. Wang, and Y. Xia, “RSC Advances,” pp. 23494–23501, 2017.

[6] M. Gorji, R. Bagherzadeh, and H. Fashandi, *21 - Electrospun nanofibers in protective clothing*. Elsevier Ltd., 2017.

[7] C. Patch, “Development of a Spirulina Extract/Alginate-Imbedded PCL Nanofibrous Cosmetic Patch,” vol. 27, no. 9, pp. 1657–1663, 2017.

[8] *No Title*. .

[9] J. Tao and S. Shivkumar, “Molecular weight dependent structural regimes during the electrospinning of PVA,” *Mater. Lett.*, vol. 61, no. 11–12, pp. 2325–2328, 2007.

[10] A. Oxides and T. Polymers, *No Title*. .

[11] Dylan Trotsek, *済無No Title No Title*, vol. 110, no. 9. 2017.

[12] K. Sarkar *et al.*, “Electrospinning to Forcespinning™,” *Mater. Today*, vol. 13, no. 11, pp. 12–14, 2010.

[13] Z.-M. Zhang, Y.-S. Duan, Q. Xu, and B. Zhang, “A review on nanofiber fabrication with

the effect of high-speed centrifugal force field," *J. Eng. Fiber. Fabr.*, vol. 14, p. 155892501986751, 2019.

[14] H. Fong, I. Chun, and D. H. Reneker, "<1-s2.0-S0032386199000683-main.pdf>," *Polymer (Guildf).*, vol. 40, no. 16, pp. 4585–4592, 1999.

[15] Y. Fang, A. D. Dulaney, J. Gadley, J. M. Maia, and C. J. Ellison, "Manipulating characteristic timescales and fiber morphology in simultaneous centrifugal spinning and photopolymerization," *Polymer (Guildf).*, vol. 73, pp. 42–51, 2015.

[16] D. De la Garza, F. De Santiago, L. Materon, M. Chipara, and M. Alcoutlabi, "Fabrication and characterization of centrifugally spun poly(acrylic acid) nanofibers," *J. Appl. Polym. Sci.*, vol. 136, no. 19, pp. 1–9, 2019.

[17] X. Zhang and Y. Lu, "Centrifugal spinning: An alternative approach to fabricate nanofibers at high speed and low cost," *Polym. Rev.*, vol. 54, no. 4, pp. 677–701, 2014.

[18] K. D. Patel *et al.*, "Coating biopolymer nanofibers with carbon nanotubes accelerates tissue healing and bone regeneration through orchestrated cell- and tissue-regulatory responses," *Acta Biomater.*, no. xxxx, 2020.

[19] C. M. Valmikinathan, J. Tian, J. Wang, and X. Yu, "Novel nanofibrous spiral scaffolds for neural tissue engineering," *J. Neural Eng.*, vol. 5, no. 4, pp. 422–432, 2008.

[20] R. James, S. G. Kumbar, C. T. Laurencin, G. Balian, and A. B. Chhabra, "Tendon tissue engineering: Adipose-derived stem cell and GDF-5 mediated regeneration using electrospun matrix systems," *Biomed. Mater.*, vol. 6, no. 2, 2011.

[21] D. Sundaramurthi, K. S. Vasanthan, P. Kuppan, U. M. Krishnan, and S. Sethuraman, "Electrospun nanostructured chitosan-poly(vinyl alcohol) scaffolds: A biomimetic extracellular matrix as dermal substitute," *Biomed. Mater.*, vol. 7, no. 4, 2012.

[22] S. Babitha and P. S. Korrapati, "Biodegradable zein – polydopamine polymeric scaffold impregnated with TiO 2 nanoparticles for skin tissue engineering Biodegradable zein – polydopamine polymeric scaffold impregnated with TiO 2 nanoparticles for skin tissue engineering," 2017.

[23] E. Shoba, R. Lakra, M. S. Kiran, and P. S. Korrapati, "Fabrication of core – shell nanofibers for controlled delivery of bromelain and salvianolic acid B for skin regeneration in wound therapeutics Fabrication of core – shell nano fi bers for controlled delivery of bromelain and salvianolic acid B for skin re."

[24] L. Huang *et al.*, “Engineered collagen – PEO nanofibers and fabrics,” vol. 5063, no. 2001, 2012.

[25] N. Bhattarai, D. Edmondson, O. Veiseh, F. A. Matsen, and M. Zhang, “Electrospun chitosan-based nanofibers and their cellular compatibility,” vol. 26, pp. 6176–6184, 2005.

[26] Z. Li *et al.*, “Enhanced energy storage performance of ferroelectric polymer nanocomposites at relatively low electric fi elds induced by surface modi fi ed BaTiO 3 nano fi bers,” vol. 164, no. May, pp. 214–221, 2018.

[27] B. Sr and T. Nano, “Liu Shaohui, Zhai Jiwei, * Wang Jinwen, Xue Shuangxi, and Zhang Wenqin,” 2014.

[28] O. S. Kwon *et al.*, “Fabrication of graphene sheets intercalated with manganese oxide/carbon nanofibers: Toward high-capacity energy storage,” *Small*, vol. 9, no. 2, pp. 248–254, 2013.

[29] L. Ji, Z. Lin, A. J. Medford, and X. Zhang, “Porous carbon nanofibers from electrospun polyacrylonitrile / SiO 2 composites as an energy storage material,” *Carbon N. Y.*, vol. 47, no. 14, pp. 3346–3354, 2009.

[30] Y. Kim, C. Hyun, M. Bok, and M. Choi, “Characteristics of electrospun PVDF / SiO 2 composite nanofiber membranes as polymer electrolyte,” *Mater. Chem. Phys.*, vol. 127, no. 1–2, pp. 137–142, 2011.

[31] N. Hyder, S. W. Lee, C. Fevzi, and P. T. Hammond, “Layer-by-Layer Assembled Polyaniline Nano fi ber / Multiwall Carbon Nanotube Thin Film Electrodes for High-Power and High-Energy Storage Applications,” no. 11, pp. 8552–8561, 2011.

[32] N. R. Dhineshbabu, G. Karunakaran, and R. Suriyaprabha, “Electrospun MgO / Nylon 6 Hybrid Nanofibers,” vol. 6, no. 1, pp. 46–54, 2014.

[33] S. Lee and S. K. Obendorf, “Use of Electrospun Nanofiber Web for Protective Textile Materials as Barriers to Liquid Penetration,” *Text. Res. J.*, vol. 77, no. 9, pp. 696–702, 2007.

[34] D. Serbezeanu, A. M. Popa, T. Stelzig, I. Sava, R. M. Rossi, and G. Fortunato, “Preparation and characterization of thermally stable polyimide membranes by electrospinning for protective clothing applications,” *Text. Res. J.*, vol. 85, no. 17, pp. 1763–1775, 2015.

[35] S. Sundarrajan and S. Ramakrishna, *The use of nanomaterials in smart protective clothing*. Woodhead Publishing Limited, 2013.

[36] "View PDF."

[37] J. Matulevicius, L. Kliucininkas, D. Martuzevicius, E. Krugly, M. Tichonovas, and J. Baltrusaitis, "Design and characterization of electrospun polyamide nanofiber media for air filtration applications," *J. Nanomater.*, vol. 2014, 2014.

[38] S. S. Rajgarhia, S. C. Jana, and G. G. Chase, "Separation of Water from Ultralow Sulfur Diesel Using Novel Polymer Nanofiber-Coated Glass Fiber Media," *ACS Appl. Mater. Interfaces*, vol. 8, no. 33, pp. 21683–21690, 2016.

[39] A. Fauzi, D. A. Hapidin, M. M. Munir, F. Iskandar, and K. Khairurrijal, "A superhydrophilic bilayer structure of a nylon 6 nanofiber/cellulose membrane and its characterization as potential water filtration media," *RSC Adv.*, vol. 10, no. 29, pp. 17205–17216, 2020.

[40] C. F. Doc, D. Simply, W. The, and F. On, "- View PDF," pp. 5–6, 2017.

[41] M. A. Hassan, B. Y. Yeom, A. Wilkie, B. Pourdeyhimi, and S. A. Khan, "Fabrication of nanofiber meltblown membranes and their filtration properties," *J. Memb. Sci.*, vol. 427, pp. 336–344, 2013.

[42] H. H. Cho, K. H. Kim, Y. A. Kang, H. Ito, and T. Kikutani, "Fine structure and physical properties of polyethylene/poly(ethene terephthalate) bicomponent fibers in high-speed spinning. I. Polyethylene sheath/poly(ethylene terephthalate) core fibers," *J. Appl. Polym. Sci.*, vol. 77, no. 10, pp. 2254–2266, 2000.

[43] M. Li, Z. Wei, and L. Jiang, "Polypyrrole nanofiber arrays synthesized by a biphasic electrochemical strategy," pp. 2276–2280, 2008.

[44] S. Zhang, "Fabrication of novel biomaterials through molecular self-assembly," vol. 21, no. 10, pp. 1171–1178, 2003.

[45] L. He *et al.*, "Fabrication and characterization of poly (L -lactic acid) 3D nanofibrous scaffolds with controlled architecture by liquid – liquid phase separation from a ternary polymer – solvent system," *Polymer (Guildf).*, vol. 50, no. 16, pp. 4128–4138, 2009.

[46] I. D. Norris, M. M. Shaker, F. K. Ko, and A. G. Macdiarmid, "Electrostatic fabrication of ultrafine conducting fibers : polyaniline r polyethylene oxide blends," pp. 109–114, 2000.

[47] S. Seidi, E. Sadat, A. Rouhollahi, and M. Baharfar, “Synthesis and characterization of polyamide-graphene oxide-polypyrrole electrospun nanofibers for spin-column micro solid phase extraction of parabens in milk samples,” *J. Chromatogr. A*, vol. 1599, pp. 25–34, 2019.

[48] G. H. Kim and W. D. Kim, “Highly porous 3D nanofiber scaffold using an electrospinning technique,” *J. Biomed. Mater. Res. - Part B Appl. Biomater.*, vol. 81, no. 1, pp. 104–110, 2007.

[49] M. Tripathi, S. Parthasarathy, and P. K. Roy, “Mechanically robust polyurea nanofibers processed through electrospinning technique,” *Mater. Today Commun.*, vol. 22, no. November 2019, p. 100771, 2020.

[50] P. Philip, E. Tomlal Jose, J. K. Chacko, K. C. Philip, and P. C. Thomas, “Preparation and characterisation of surface roughened PMMA electrospun nanofibers from PEO - PMMA polymer blend nanofibers,” *Polym. Test.*, vol. 74, no. January, pp. 257–265, 2019.

[51] C. C. Liao, C. C. Wang, and C. Y. Chen, “Stretching-induced crystallinity and orientation of polylactic acid nanofibers with improved mechanical properties using an electrically charged rotating viscoelastic jet,” *Polymer (Guildf).*, vol. 52, no. 19, pp. 4303–4318, 2011.

[52] J. Li, Y. Hu, H. Qiu, G. Yang, S. Zheng, and J. Yang, “Coaxial electrospun fibres with graphene oxide/PAN shells for self-healing waterborne polyurethane coatings,” *Prog. Org. Coatings*, vol. 131, no. 516, pp. 227–231, 2019.

[53] A. Olusegun *et al.*, “We are IntechOpen , the world ’ s leading publisher of Open Access books Built by scientists , for scientists TOP 1 %,” *Intech*, vol. i, no. tourism, p. 38, 2012.

[54] M. M. M. G. P. G. Mantilaka, R. T. De Silva, S. P. Ratnayake, G. Amaratunga, and K. M. N. de Silva, “Photocatalytic activity of electrospun MgO nanofibres: Synthesis, characterization and applications,” *Mater. Res. Bull.*, vol. 99, no. November 2017, pp. 204–210, 2018.

[55] A. Demir, B. Acikabak, and Z. Ahan, “Development of Carbon Nanofiber Yarns by Electrospinning,” *IOP Conf. Ser. Mater. Sci. Eng.*, vol. 460, no. 1, 2018.

[56] Y. Lu *et al.*, “Parameter study and characterization for polyacrylonitrile nanofibers fabricated via centrifugal spinning process,” *Eur. Polym. J.*, vol. 49, no. 12, pp. 3834–3845, 2013.

[57] C. Chen, M. Dirican, and X. Zhang, *SPINNING d HIGH RATE*. Elsevier Inc., 2019.

[58] S. Padron, A. Fuentes, D. Caruntu, and K. Lozano, “Experimental study of nanofiber production through forcespinning,” *J. Appl. Phys.*, vol. 113, no. 2, pp. 1–9, 2013.

[59] Y. Lu *et al.*, “Centrifugal spinning: A novel approach to fabricate porous carbon fibers as binder-free electrodes for electric double-layer capacitors,” *J. Power Sources*, vol. 273, pp. 502–510, 2015.

[60] E. Stojanovska, M. Kurtulus, A. Abdelgawad, Z. Candan, and A. Kilic, “Developing lignin-based bio-nanofibers by centrifugal spinning technique,” *Int. J. Biol. Macromol.*, vol. 113, pp. 98–105, 2018.

[61] L. D. Cremar, J. Acosta-Martinez, A. Villarreal, A. Salinas, and K. Lozano, “Mechanical and electrical characterization of carbon nanofibers produced from water soluble precursors,” *Mater. Today Commun.*, vol. 7, pp. 134–139, 2016.

[62] L. Ren, R. Ozisik, S. P. Kotha, and P. T. Underhill, “Highly efficient fabrication of polymer nanofiber assembly by centrifugal jet spinning: Process and characterization,” *Macromolecules*, vol. 48, no. 8, pp. 2593–2602, 2015.

[63] N. A. S. Gundogdu, Y. Akgul, and A. Kilic, “Optimization of centrifugally spun thermoplastic polyurethane nanofibers for air filtration applications,” *Aerosol Sci. Technol.*, vol. 52, no. 5, pp. 515–523, 2018.

[64] M. Krifa, M. A. Hammami, and H. Wu, “Occurrence and morphology of bead-on-string structures in centrifugal forcespun PA6 fibers,” *J. Text. Inst.*, vol. 106, no. 3, pp. 284–294, 2015.

[65] Y. Lu *et al.*, “Parameter study and characterization for polyacrylonitrile nanofibers fabricated via centrifugal spinning process,” *Eur. Polym. J.*, vol. 49, no. 12, pp. 3834–3845, 2013.

[66] H. Hosseinian, A. Valipouri, S. A. Hosseini Ravandi, and A. Alirezazadeh, “Determining the effect of centrifugal and electrical forces on the jet behaviors, the nanofiber structure, and morphology,” *Polym. Adv. Technol.*, vol. 30, no. 4, pp. 941–950, 2019.

[67] M. Kancheva, A. Toncheva, N. Manolova, and I. Rashkov, “Advanced centrifugal electrospinning setup,” *Mater. Lett.*, vol. 136, pp. 150–152, 2014.

[68] M. A. Hammami, M. Krifa, and O. Harzallah, “Centrifugal force spinning of PA6 nanofibers - processability and morphology of solution-spun fibers,” *J. Text. Inst.*, vol. 105, no. 6, pp. 637–647, 2014.

[69] C. A. Ramírez-Herrera, H. Gonzalez, F. de la Torre, L. Benitez, J. Cabañas-Moreno, and K. Lozano, “Electrical properties and electromagnetic interference shielding effectiveness of interlayered systems composed by carbon nanotube filled carbon nanofiber mats and polymer composites,” *Nanomaterials*, vol. 9, no. 2, pp. 1–19, 2019.

[70] Y. Wang, W. Lu, Y. Wang, T. Xu, and W. Chen, “Interpenetrating-Syncretic Micro-Nano Hierarchy Fibers for Effective Fine Particle Capture,” *Adv. Eng. Mater.*, vol. 1801361, no. 2, pp. 1–12, 2019.

[71] L. Ren, R. Ozisik, and S. P. Kotha, “Rapid and efficient fabrication of multilevel structured silica micro-/nanofibers by centrifugal jet spinning,” *J. Colloid Interface Sci.*, vol. 425, pp. 136–142, 2014.

[72] X. Liu, B. Jiang, X. Yin, H. Ma, and B. S. Hsiao, “Highly permeable nanofibrous composite microfiltration membranes for removal of nanoparticles and heavy metal ions,” *Sep. Purif. Technol.*, vol. 233, no. July 2019, p. 115976, 2020.

[73] M. Erceg, “Thermochimica Acta Kinetic analysis of thermal degradation of poly (ethylene glycol) and poly (ethylene oxide) s of different molecular weight,” vol. 498, pp. 71–80, 2010.

[74] L. Wang, Z. Ahmad, J. Huang, J. Li, and M. Chang, “Multi-compartment centrifugal electrospinning based composite fi bers,” *Chem. Eng. J.*, vol. 330, no. May, pp. 541–549, 2017.

[75] W. M. Chang, C. C. Wang, and C. Y. Chen, “Fabrication of ultra-thin carbon nanofibers by centrifuged-electrospinning for application in high-rate supercapacitors,” *Electrochim. Acta*, vol. 296, pp. 268–275, 2019.

[76] B. H. Stuart, “VIBRATIONAL CTROSO) In / Polymer crystallinity studied using Raman spectroscopy,” vol. 10, pp. 79–87, 1996.

[77] W. S. Khan, M. Ceylan, L. Saeednia, and R. Asmatulu, “Chemical and thermal investigations of electrospun polyacrylonitrile nanofibers incorporated with various nanoscale inclusions CHEMICAL AND THERMAL INVESTIGATIONS OF ELECTROSPUN POLYACRYLONITRILE NANOFIBERS INCORPORATED WITH VARIOUS,” no. May, 2017.

[78] M. K. Ozturk, B. Nergis, and C. Candan, “Thermal Analysis of PVA Nanofibrous Membranes,” 2018.

[79] B. Raghavan, H. Soto, and K. Lozano, “Fabrication of melt spun polypropylene nanofibers by Forcespinning,” *J. Eng. Fiber. Fabr.*, vol. 8, no. 1, pp. 52–60, 2013.

[80] S. Yang, J. Taha-tijerina, K. Hernandez, and K. Lozano, “Dynamic mechanical and thermal analysis of aligned vapor grown carbon nanofiber reinforced polyethylene,” vol. 38, pp. 228–235, 2007.

[81] R. Nayak, I. Louis, G. Peeters, M. O. Shea, and L. Nichols, “Fabrication and characterisation of polypropylene nanofibres by meltblowing process using different fluids,” pp. 273–281, 2013.

BIOGRAPHY SKETCH

Omosola Oriretan, had his bachelor's degree in industrial chemistry from Federal University of Technology, Akure Ondo State, Nigeria. After his undergraduate degree he worked as Chemist, Research and Development Chemist and Quality Control Manager in the Pharmaceutical, Chemical, Paints and Coatings industries. He researched, developed and formulated different categories of coatings from the Emulsion paints to High performance industrial Coatings.

He left Nigeria for United states of America having been awarded the prestigious Presidential Graduate Research Assistant scholarship to study where he earned a master's degree in chemistry from University of Texas Rio Grande Valley, Edinburg, Texas in December 2020.

Contact: oriretan.omosola@gmail.com